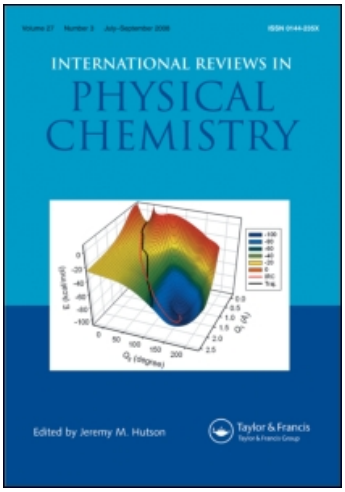


**International Reviews in Physical Chemistry**
Publication details, including instructions for authors and subscription information:
http://www.informaworld.com/smpp/title~content=t713724383

# Reactions of some [C, N, O]-containing molecules with Si surfaces: Experimental and theoretical studies

Xin Lu; M. C. Lin

Online publication date: 26 November 2010

**To cite this Article** Lu, Xin and Lin, M. C.(2002) 'Reactions of some [C, N, O]-containing molecules with Si surfaces: Experimental and theoretical studies', International Reviews in Physical Chemistry, 21: 1, 137 — 184
**To link to this Article: DOI:** 10.1080/01442350110109658
**URL:** http://dx.doi.org/10.1080/01442350110109658

INT. REVIEWS IN PHYSICAL CHEMISTRY, 2002
VOL. 21, NO. 1, 137–184

Taylor & Francis
Taylor & Francis Group

# Reactions of some [C, N, O]-containing molecules with Si surfaces: experimental and theoretical studies

XIN LU† and M.C. LIN‡

† State Key Laboratory for Physical Chemistry of Solid Surfaces and Department of Chemistry, Xiamen University, Xiamen 361005, China

‡ Department of Chemistry, Emory University, Atlanta, Georgia 30322, USA

Mechanistic understanding of the reactions of small molecules containing C, N and O with Si surfaces is not only fundamentally interesting but also practically important to the development of SiC, SiN, SiO, SiCN and diamond thin films. This article reviews the recent experimental and theoretical work on the reactions of a dozen of [C, N, O]-containing molecules with single-crystal surfaces of Si, including N precursors (ammonia ($NH_3$), hydrazine ($N_2H_4$) and hydrazoic acid ($HN_3$)), CO-containing molecules (carbon monoxide (CO), formaldehyde ($CH_2O$), acetaldehyde ($CH_3CHO$), formic acid (HCOOH), methanol ($CH_3OH$) and ketene ($CH_2CO$)), CN-containing molecules (hydrogen cyanide (HCN), cyanogen ($C_2N_2$), acetonitrile ($CH_3CN$) and methylhydrazine ($CH_3N_2H_3$)), a CNO-containing molecule (formamide ($NH_2CHO$)) and some aromatic heterocyclic compounds (pyrrole ($C_4H_5N$), thiophene ($C_4H_4S$), furan ($C_4H_4O$), pyridine ($C_5H_5N$), pyrazine ($C_4H_4N_2$) and *s*-triazine ($C_3H_3N_3$)).



## Contents



*International Reviews in Physical Chemistry* ISSN 0144–235X print/ISSN 1366–591X online 
http://www.tandf.co.uk/journals
DOI: 10.1080/01442350110109658

## 1. Introduction

Mechanistic understanding of the reactions of small molecules containing C, N and O with Si surfaces is not only fundamentally interesting but also practically important to the chemistry of SiX (X = C, N, O or CN) and diamond thin-film deposition. On the one hand, the study of small molecules on the Si surfaces provides useful information for the establishment of Si surface chemistry [1–5]. On the other hand, numerous small [C, N, O]-containing molecules serve as simple molecular precursors for the formation of SiC, SiN, SiO, SiCN and diamond thin films on Si surfaces [6, 7]. On account of the ubiquitous role of Si in microelectronic technology, much effort has been made in this field in the past two decades. So far several review articles have been published regarding the chemical modification of Si surfaces [1–7], most of them focusing on the controlled monolayer functionalization of Si surfaces

by chemical attachments of alkenes and the related organic compounds through Si–C bonds [1–5]. In recent years, much attention has been paid in an effort to search for good precursors for the production of SiX thin films. For this purpose, the reactions of a number of inorganic and organic molecules, which can potentially be employed as precursors for deposition of these films, with the two representative Si crystal surfaces, that is the reconstructed Si(100)-$2 \times 1$ and Si(111)-$7 \times 7$ surfaces, have been studied experimentally and theoretically in the laboratory [7–37]. The results of these fundamental studies, some of which are yet to be published, as well as those of the relevant experimental and theoretical studies reported by other researchers are reviewed herein. The small molecules concerned are N precursors (ammonia ($NH_3$), hydrazine ($N_2H_4$) and hydrazoic acid ($HN_3$)), CO-containing molecules (carbon monoxide (CO), formaldehyde ($CH_2O$), acetaldehyde ($CH_3CHO$), formic acid (HCOOH), methanol ($CH_3OH$) and ketene ($CH_2CO$)), CN-containing molecules (hydrogen cyanide (HCN), cyanogen ($C_2N_2$), acetonitrile ($CH_3CN$) and methylhydrazine ($CH_3N_2H_3$)), a CNO-containing molecule (formamide ($NH_2CHO$)) and some aromatic heterocyclic compounds (pyrrole ($C_4H_5N$), thiophene ($C_4H_4S$), furan ($C_4H_4O$), pyridine ($C_5H_5N$), pyrazine ($C_4H_4N_2$) and s-triazine ($C_3H_3N_3$)).



## 2. Geometries and electronic structures of the reconstructed Si(100)-$2 \times 1$ and Si(111)-$7 \times 7$ surfaces

Two representative single-crystal surfaces of Si, namely the reconstructed Si(100)-$2 \times 1$ and Si(111)-$7 \times 7$ surfaces [38, 39], have been intensively studied. Before reviewing in detail the reactions on these single crystal Si surfaces, we would like to present some essential aspects of the geometry and electronic structure of these surfaces.

### 2.1. *Si(100)*

Upon annealing at high temperatures, the Si(100) surface reconstructs to give the $(2 \times 1)$ structure, in which adjacent surface atoms pair into dimers, as shown in figure 1(*a*). The bonding within the surface dimers can be formally described in terms of a $\sigma$ bond and a $\pi$ bond, analogous to the C=C double bonds of alkenes [39]. However, owing to the large Si–Si distance and the bending back bonds that connect the surface dimer with the bulk atoms, the $\pi$ bond within the Si–Si dimer is quite weak and, in some cases, might be regarded as a diradical [40]. In a more complicated manner, the dimers in the real case were observed to tilt, giving rise to c$(4 \times 2)$ symmetry or p$(2 \times 2)$ symmetry [41–43]. The dimer tilting is accompanied by a charge transfer from the buckled-down atom to the buckled-up atom, which adds zwitterionic character to the dimers [44]. Sophisticated quantum-chemical calculations [45, 46] showed that one of the major factors which controls dimer tilting is the electron correlation effect. It is likely that none of the above models gives perfect descriptions of the bonding with the dimers at the Si(100)-$2 \times 1$ surface, but rather that the bonding has characteristics of all three models. Nevertheless, such unique bonding motifs arm the Si(100)-$2 \times 1$ surface with unique chemical reactivity towards a wide variety of inorganic and organic molecules, especially to those unsaturated organic compounds such as alkenes and alkynes [1–5]. Needless to say, a mechanistic understanding of the unique chemistry of the Si(100)-$2 \times 1$ surface is of great importance to microelectronics manufacturing.

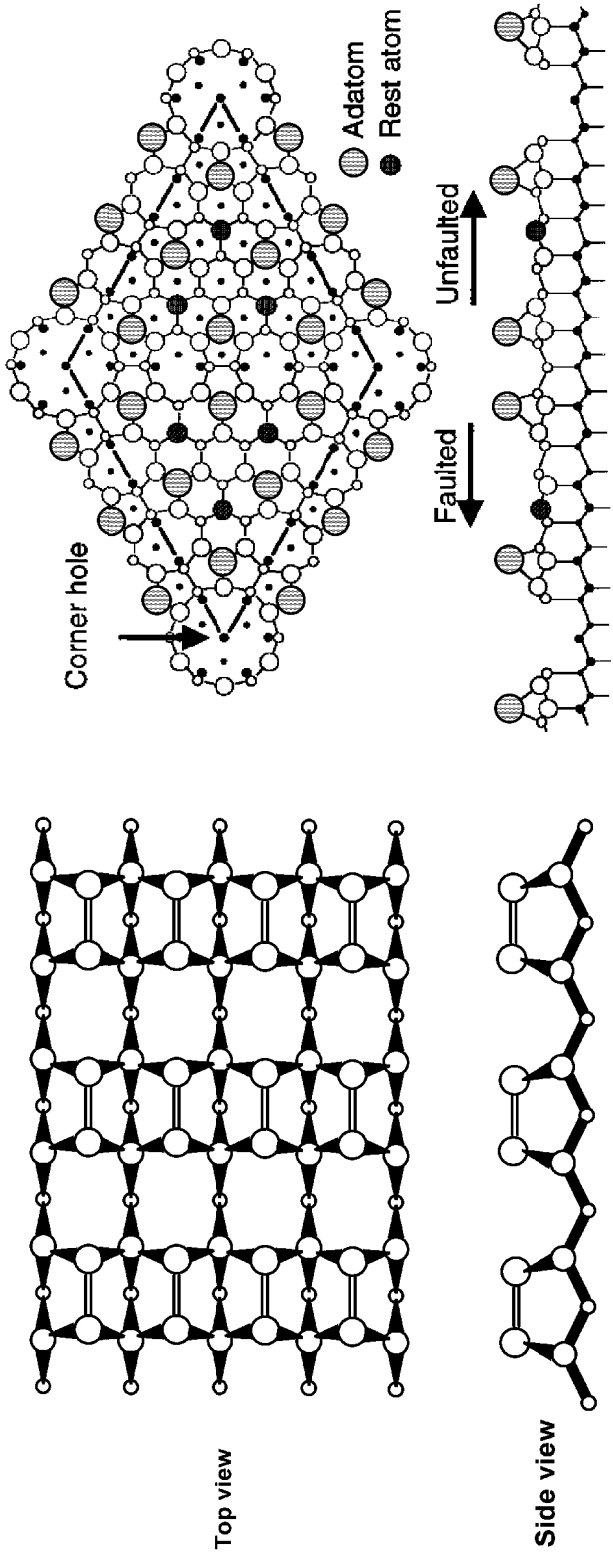


Figure 1. Structure models of (*a*) the reconstructed Si(100)-$2 \times 1$ surface and (*b*) the reconstructed Si(111)-$7 \times 7$ surface. (From [38]. Reproduced by the permission of the American Institute of Physics.)

### 2.2. *Si(111)*

The thermodynamically most stable crystal surface of Si is the reconstructed Si(111)-7 × 7 surface, which adopts the dimer–adatom–stacking-fault (DAS) structure proposed by Takayanagi *et al.* [38], as shown in figure 1(*b*). The intriguing 7 × 7 reconstruction provides an array of chemically non-equivalent atoms in the topmost layers of atoms, resulting in a rich variety of chemically interesting and spatially inhomogeneous chemical sites. As shown in figure 1(*b*), the large (7 × 7) surface unit cell contains seven chemically distinguishable types of surface atom. There are three corner adatoms, three centre adatoms and three rest atoms at both the faulted and the unfaulted halves as well as one rest atom at the bottom of deep corner hole. Accordingly, the 19 dangling bonds present within a (7 × 7) surface unit cell are available for chemical reaction, 12 of which are located at topmost adatoms, six at the rest atoms and one at the corner hole atom in the fourth layer. Theoretically it was predicted that charge transfer occurs preferentially from the adatoms to the rest atoms [47, 48], thereby resulting in completely occupied dangling bonds at the rest atoms and the corner hole atoms as well as partially occupied or empty dangling bonds at the adatoms. Such intriguing charge transfer was confirmed by scanning tunnelling microscopy (STM) observations [43, 49, 50]. STM topographs obtained at sample bias voltages of from +0.8 to +2.0 V (probing unoccupied states) showed clearly the 12 adatoms in the (7 × 7) unit cell. More elaborate tunnelling spectra revealed the dangling-bond states associated with adatoms at 0.35 eV below $E_F$ and the dangling-bond states associated with rest atoms at 0.8 eV below $E_F$ [43, 49]. It is expected that the chemical reactivity of the Si(111)-(7 × 7) is inherently related to the inhomogeneous dangling bond states present on the very surface.



## 3. The reactions of N precursors

Nitrogen hydrides, such as ammonia ($NH_3$) and hydrazine ($N_2H_4$), are useful as N precursors for the formation of Si nitride films. In addition, $HN_3$ was proven to be a potential precursor for the production of Si nitride films. In this section, the reactions of these three N precursors with Si(100)-2 × 1 and Si(111)-7 × 7 surfaces are reviewed.

### 3.1. *$NH_3$/Si(100)*

Among the three N precursors concerned, $NH_3$ has been most extensively studied both experimentally and theoretically [51–73]. Earlier studies, using ion scattering spectroscopy and X-ray photoelectron spectroscopy (XPS), reported that ammonia dissociated on the Si(100) surface at 90 K and the chemisorbed H terminated the dangling bonds while N occupied subsurface sites [51, 52]. Ion scattering experiments detected only surface H(a) and Si after heating to 220 K. On the other hand, Hlil *et al.* [53], on the basis of their XPS and ultraviolet photoelectron spectroscopy (UPS) results, reported that $NH_x$ species were produced on the Si(100) surface after $NH_3$ adsorption at 100 K. They also suggested that the saturation coverage of $NH_3$ on the surface is one molecule per two Si dimers. The $NH_x$ species were later assigned to >NH(a) using XPS and UPS [54, 55]. At temperatures between 80 and 300 K, most experimental studies such as isotope mixing [56], electron-stimulated desorption ion-angular distribution (ESDIAD) [57], XPS [58], UPS [59] and high-resolution electron-energy-loss spectroscopy (HREELS) [60, 61] suggested that $NH_2$(a) and H(a) are the major species produced upon adsorption of ammonia on Si(100)-2 × 1.

Based on their temperature-programmed desorption (TPD) and ESDIAD results, Yates and co-workers [56, 57] reported, firstly, that the saturation coverage of $NH_3$ on the surface is one $NH_3$ molecule per Si dimer, secondly, that $NH_3$ adsorbs dissociatively on one dimer, and, thirdly, that the $NH_2$(a) species chemisorbed to the Si dimer atoms via a single Si–N bond at 120 K. The high-resolution electron-energy-loss spectra showed the $\delta_s(NH_2)$ scissor mode between 1550 and 1575 $cm^{-1}$ and the $\nu$(Si–H) stretching mode between 2070 and 2080 $cm^{-1}$, positively identifying $NH_2$(a) and H(a) as products of $NH_3$ adsorption on the Si(100)-2 × 1 surface.

The mechanism of the $NH_3$ adsorption process on the Si(100)-2 × 1 surface has also received intensive attention from the theoretical side. The pioneering discrete variational $X_\alpha$ (DV-$X_\alpha$) and semiempirical cluster model calculations based on atom superposition and electron delocalization–molecular orbital theory [63] predicted that the dissociative adsorption of $NH_3$ on the surface is across the dimer rows. Carter and coworkers [64] reported the dissociative adsorption of $NH_3$ on a single Si dimer ($Si_9H_{12}$) using the complete-active-space self-consistent field–multireference single and double excitation configuration interaction level of theory. Their results agree with the experimental finding of Yates and co-workers [56, 57] that one $NH_3$ molecule adsorbs dissociatively on to a single Si dimer and has been later confirmed by the very recent density functional theory (DFT) slab model calculations [65–68] and DFT cluster model calculations [69–74].



We have recently performed density functional cluster model calculations to understand the mechanism for the adsorption and desorption of $NH_3$ on the Si(100)-2 × 1 system [74]. The profile of the energy surface predicted at the B3LYP/6-31G(d) level [75–77] and at the two-layered ONIOM(coupled cluster singles plus doubles with perturbative triples (CCSD(T)/6-31G(d):B3LYP/6-31G(d))) level [16, 77, 78] using the single-dimer $Si_9H_{12}$ cluster model is depicted in figure 2. Our result shows that the dissociation of $NH_3$ on a single dimer is barrierless, but via a molecular precursor state and a transition state for N–H cleavage. Apart from the dissociation on a single dimer, the dissociation across two dimers has also been considered using the double-dimer $Si_{15}H_{16}$ surface model and were also shown to be barrierless, but via a transition state which is 11.2 kcal $mol^{-1}$ (predicted at the B3LYP/6-31G(d) level) higher in energy than the transition state for dissociation over a single dimer. Furthermore, adsorbate–adsorbate interaction and its effect on desorption energy were investigated and the results suggested that the coverage effect on the desorption energy is non-negligible.

In addition, kinetic modelling of the thermal desorption of $NH_3$ on Si(100)-2 × 1 was carried out by employing the canonical variational Rice–Ramsperger–Kassel–Marcus (RRKM) theory [79] with the computed energetics and transition state structures [74]. The calculations were performed with the RRKM programs for systems involving two quantum wells, each having one or two exit product channels [80–82]. The use of the energetics predicted at the ONIOM(CCSD(T)/6-31G(d):B3LYP/6-31G(d)) level for $NH_2(a) + H(a)$ adsorption gave rise to the rate constant for associative desorption, $k_{NH_2+H} = 4.59 \times 10^{13} \exp(-45\,300/RT)\ s^{-1}$, in good agreement with the experimental value [57], $k_{NH_2+H} = 1 \times 10^{14} \exp(-46\,000/RT)\ s^{-1}$. The initial sticking probability for $NH_3$ adsorption in the temperature range 330–590 K was also calculated and compared with the experimental measurements reported by Takaoka and Kusinoki [62]. The theoretical initial sticking probabilities at different temperatures obtained by using the B3LYP

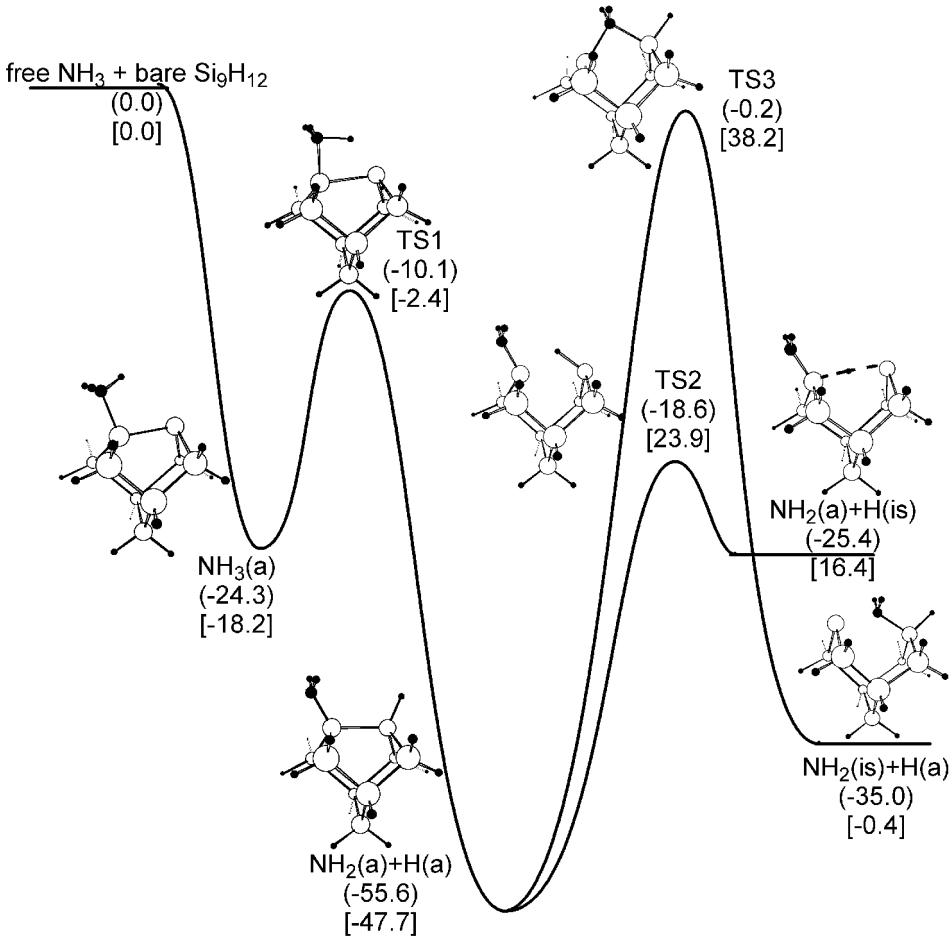


Figure 2. The profile of energy surfaces for the $NH_3/Si_9H_{12}$ model system predicted at the B3LYP/6-31G(d) level of theory. The energies (in kilocalories per mole) given in square brackets are predicted by means of two-layered ONIOM(CCSD(T):B3LYP) calculations.

energetics and the ONIOM energetics are demonstrated in figure 3, together with the experimental data. The theoretical sticking probability based on the B3LYP energetics is apparently overestimated, owing to the deeper well depths predicted at the B3LYP/6-31G(d) level. However, good agreement is reached between the theoretical sticking probability based on ONIOM energetics and the experimental measurements [62]. This work therefore provides a successful example of using the statistical theory that was derived for gas-phase reactions to treat gas–surface reactions.

### 3.2. *$NH_3$/Si(111)*

The interaction of $NH_3$ with the Si(111)-$7 \times 7$ surface is more intriguing and complicated than its interaction with the Si(100) surface. A number of studies using various surface-sensitive techniques have been performed on the adsorption of $NH_3$

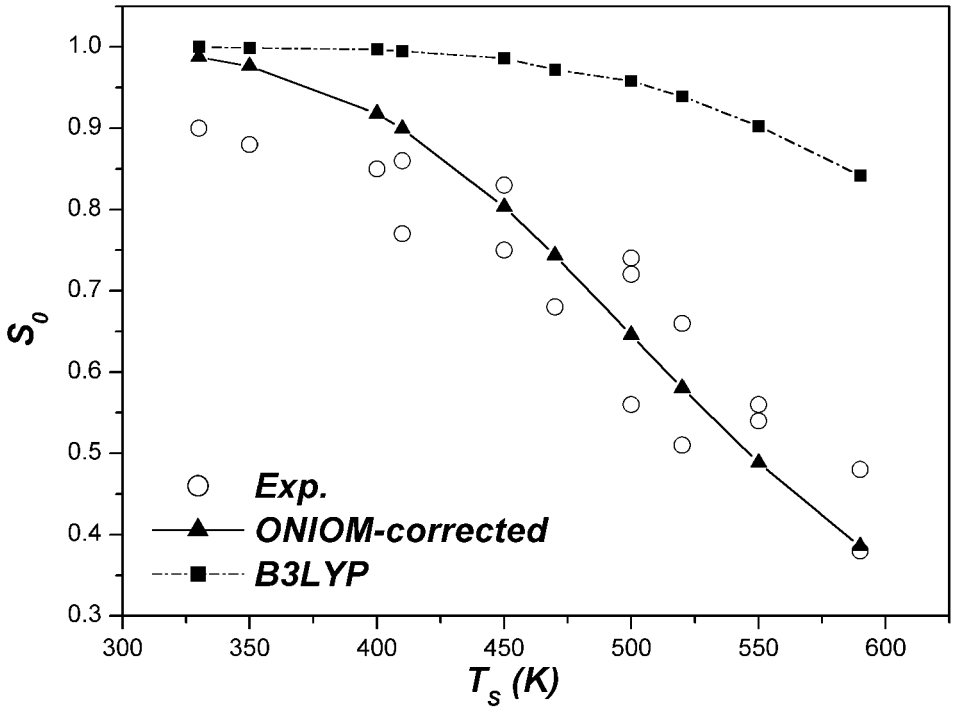


Figure 3. Theoretical and experimental data of the initial sticking probability for $NH_3$ adsorption on the Si(100)-$2 \times 1$ surface.



on the Si(111) surfaces [50, 54, 55, 58, 83–100], from the early electron-energy-loss spectroscopy (EELS) study by Nishijima and Fujihara [83] to the elaborate STM study by Wolkow and Avouris [50] and the most recent photoemission measurements by Björkqvist *et al.* [100]. The HREELS, UPS, XPS experiments [93, 94, 100] showed that, at low temperatures, $NH_3$ was dissociatively adsorbed on the Si(111) substrate, giving rise to $NH_2$, NH and H adspecies. In their STM study, Wolkow and Avouris [50] observed striking spatial variation in the reactivity of surface dangling bond states towards $NH_3$, that is the Si rest atoms are the most reactive followed by the centre adatoms and then by the corner adatoms. In the STM topographs, half of the adatoms appeared dark at a bias voltage of 0.8 V upon $NH_3$ adsorption and became bright at a bias voltage of 3 V, and the dark centre adatoms are more than twice in number than the dark corner adatoms [50]. This phenomenon revealed the variation in adatom reactivity, that is the centre adatoms are more reactive than the corner adatoms, as well as the preservation of the $(7 \times 7)$ surface reconstruction during $NH_3$ adsorption. More elaborate tunnelling spectroscopy measurements indicated that, upon $NH_3$ reaction, the characteristic state at $-0.8$ eV due to the dangling bond at a Si rest atom was eliminated immediately; meanwhile, the surface states at a reacted adatom were also eliminated. Despite the large number of experimental studies, the only consensus that has been reached so far regarding $NH_3$ adsorption on the Si(111)-$7 \times 7$ surface is simply that $NH_3$ is dissociatively adsorbed over a rest-atom–adatom pair site, resulting in $NH_2$(a) and H(a) adspecies. One major controversy is on which site the dissociative adsorption of $NH_3$ is initiated. While some of the photoemission experiments advocated the

adatoms [100], the STM experiments and a core-level photoemission experiment [50, 99] suggested the rest atoms. Similar controversy exists prevalently in the studies of the dissociative chemisorption of XH ($X = CH_3O$, HO or HS) molecules on the same surface.

Theoretical study of this intriguing chemisorption system is scarce, probably owing to the complexity of the Si(111)-$(7 \times 7)$ surface in geometric and electronic structures. Ezzehar *et al.* [101] reported a semiempirical extended Hückel theory study of the initial stage of $NH_3$ adsorption on this surface. Based on the calculated adsorption energies, they concluded that the homolytic dissociation of $NH_3$ on a pair of adatoms is the most favourable, followed by the adsorption on a rest-atom–adatom pair site. Such a prediction, however, is in contradiction with the experimental inference [50, 100] that both the adatom and the rest atom be involved in the initial stage of $NH_3$ adsorption. In addition, their calculations showed that the double dissociation of $NH_3$ into NH and two H adspecies is favourable, and the most likely geometry adopted by NH species is bridging over an adatom and one of its backbone atoms.

We have recently performed DFT cluster model calculations to explore the mechanism for the dissociative adsorption of $NH_3$ on the Si(111)-$7 \times 7$ surface [37]. A $Si_{16}H_{18}$ surface model has been used to represent a rest-atom–adatom pair site at the faulted half of the Si(111)-$7 \times 7$ unit cell. Figure 4 gives the optimized geometries for the intermediates, transition states and products of the $NH_3$ dissociation. The profile of the energy surface is presented in figure 5. The calculations revealed the following.



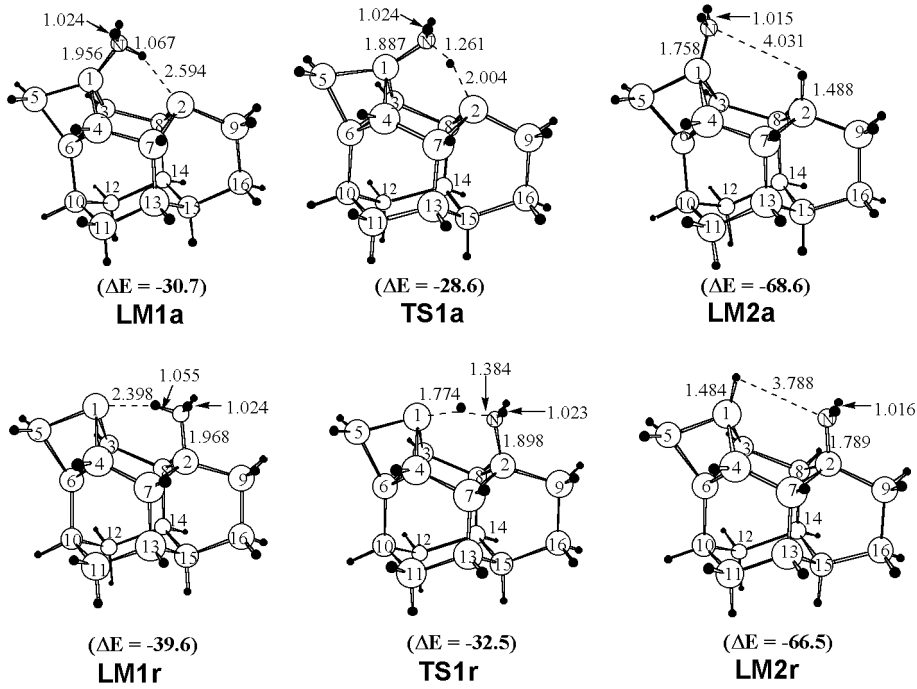


Figure 4. B3LYP-optimized geometries for the stationary points of the $NH_3/Si_{16}H_{18}$ model system (Si, H, LANL2DZ; N, 6-31+G(d)). $\Delta E$ is given in kilocalories per mole.

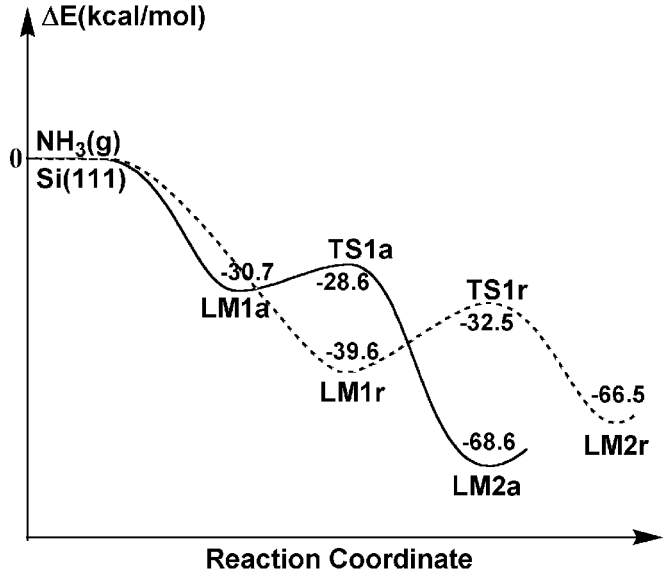


Figure 5. Profile of energy surfaces for the dissociative adsorption of $NH_3$ on the $Si_{16}H_{18}$ surface model. The reported energies are zero-point energy uncorrected.

(i) The dissociation of $NH_3$ can be initiated in a barrierless manner either over an adatom or on a rest atom.
(ii) On either surface site, the dissociation proceeds via a molecular precursor state and a transition state, producing $NH_2$ and H adspecies without thermal activation.
(iii) The molecular precursor states, LM1a on the adatom site and LM1r on the rest-atom site, are metastable and, hence, can hardly be detected experimentally.

A surprising prediction of this study is the lack of a site preference during the initial stage of $NH_3$ adsorption, as previously found in experiments, although controversially the study advocated a site preference of $NH_3$ adsorption. In addition, the barrierless adsorption of $NH_3$ initiated over a rest atom site is seemingly in contradiction with chemical intuition, as the dangling bond at a rest-atom was believed to be completely occupied owing to the preferential charge transfer from the centre adatom to the rest atom [47, 48, 102, 103] and, thus, would be repulsive to the lone-pair electrons at the N atom of the incoming $NH_3$ molecule. Wolkow and Avouris [50] proposed a reverse charge transfer from the rest atom to the adatom to interpret their STM observation of the superior reactivity of the rest atoms to that of the adatoms. Whether the charge transfer is facile or not is a question that is not yet solved and deserves further theoretical study. For this purpose, natural bond orbital (NBO) analyses [104] on the Kohn–Sham wavefunctions of the model system at selected Si–N distances were performed, the results of which are listed in table 1. For a free surface model, the dangling-bond states at the adatom and the rest atom are predicted to have eigenvalues of −0.0797 and −0.11526 au respectively, in agreement with the STM observation [50] that the dangling-bond states at adatoms are higher in energy than the dangling-bond states at rest atoms. The dangling-bond orbital

Table 1. Occupation and orbital energy of the dangling bond states at difference $H_3N$–Si distances predicted by NBO analyses.

| | | Dangling bond at adatom | | Dangling bond at rest atom | |
|---|---|---|---|---|---|
| | $R$(Si–N) (Å) | Occupation ($e$) | Energy (au) | Occupation ($e$) | Energy (au) |
| Free-surface model | | 0.78 | −0.079 7 | 0.93 | −0.115 26 |
| $H_3N \rightarrow$ rest atom | 3.4 | 1.79 | −0.267 29 | 0.55 | −0.134 56 |
| | 3.1 | 1.86 | −0.262 90 | 0.48 | −0.137 86 |
| LM1r | 1.97 | 1.89 | −0.257 99 | — | — |
| $H_3N \rightarrow$ adatom | 3.4 | 0.57 | −0.078 76 | 1.24 | −0.091 22 |
| | 3.1 | 0.54 | −0.084 11 | 1.71 | −0.224 22 |
| LM1a | 1.96 | — | — | 1.78 | −0.211 56 |



occupation is 0.78$e$ at the adatom and 0.97$e$ at the rest atom. When an ammonia molecule approaches the rest atom with its N end, the charge transfer from the rest atom to the adatom is found to be surprisingly great, even at a very large Si–N distance (e.g. 3.4 Å). At a Si–N distance of 3.4 Å, the dangling-bond orbital occupation at the adatom increases to 1.79$e$ from 0.78$e$ for the free-surface model and, meanwhile, the dangling-bond occupation decreases to 0.55$e$ from 0.93$e$ for the free-surface model, indicating the facile charge transfer over the dangling bond states induced by the weak interaction of a foreign molecule. Upon formation of the metastable molecular adsorption state LM1r, the dangling-bond state at the rest atom diminishes, while the dangling-bond orbital at the adatom has an occupation of 1.89$e$. Similar charge transfer is observed in the process of $NH_3$ approaching the adatom with its N end. Similar charge transfer is observed in the process of $NH_3$ approaching the adatom with its N end. The above theoretical analyses thus provide the first theoretical evidence of the high charge flexibility of the dangling-bond states on the Si(111)-7 × 7 surface, which is of great significance to our understanding of the chemistry of the technologically important Si surfaces.

### 3.3. *$N_2H_4$/Si(100)*

The reactivity of $N_2H_4$ on the Si(100)-2 × 1 surface was studied by using XPS, UPS, HREELS and low-energy electron diffraction (LEED) techniques [8]. Upon adsorption of $N_2H_4$ at a dosage of 0.2 langmuirs (L) on the surface at 100 K, partial dissociation of the NH bonds was indicated by the appearance of the Si–H stretching mode at 255 meV in HREELS and the 399.0 eV peak in XPS, which was assigned to the $N_2H_x$ (presumably $N_2H_3$) species. This behaviour is similar to the dissociative adsorption of $NH_3$ on the same surface. At higher dosages ($D > 0.4$ L), H bonding was noted to be formed in the overlayer adsorbates. The NH bond breaking continued as the sample was annealed at higher temperatures. Above 600 K, NN bond cleavage occurred and the product $NH_x$ ($x = 0, 1, 2$) species were identified on the surface. This was evidenced by the disappearance of the NN stretching mode in HREELS. Further annealing the surface to $T_s > 800$ K caused the complete dissociation of the NN and NH bonds and the desorption of $H_2$, while atomic N remained on the surface to form silicon nitride. Based on their experimental results,

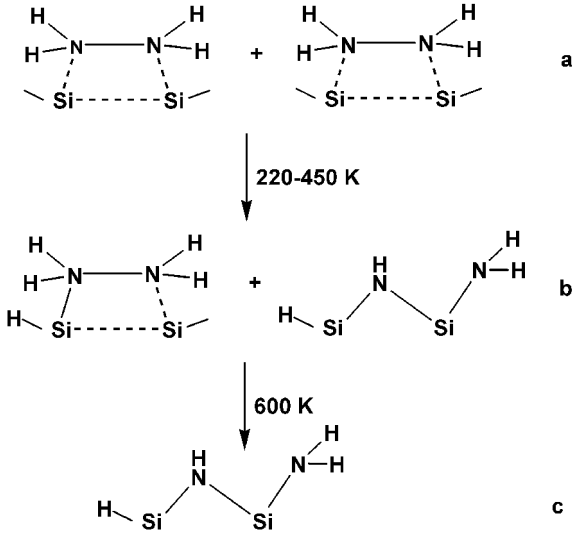


Figure 6. The proposed model for the adsorption geometry of $N_2H_4$ on the Si(100)-$2 \times 1$ surface at different temperatures. (From [8]. Reproduced by the permission of Elsevier Science.)



Bu and Lin [8] proposed the following model for the adsorption geometry of $N_2H_4$ on the Si(100)-$2 \times 1$ surface at different temperature, as shown in figure 6.

While theoretical confirmation of the aforementioned model of adsorption geometry is lacking, a recent STM study reported by Tindall *et al.* [105, 106] provided evidence supporting this model. The STM images showed that at room temperature the predominant pathway for $N_2H_4$ adsorption on Si(100) is across the Si dimers with the N-N bond parallel to the surface [105, 106]. Theoretical modelling of the initial state of $N_2H_4$ adsorption on the Si(100)-$2 \times 1$ is being performed by Luo and Lin [107]. Preliminary results revealed that, similar to the dissociative adsorption of $NH_3$, the dissociative adsorption of $N_2H_4$ over a surface Si dimer is barrierless, producing Si-$N_2H_3$ and Si-H surface species. Further theoretical study is in progress regarding the possible dissociation pathways starting from the thus-formed Si-$N_2H_3$ surface species.

### 3.4. *$N_2H_4$/Si(111)*

The adsorption and thermal decomposition of $N_2H_4$ on the Si(111)-$7 \times 7$ surface were investigated using XPS, UPS and HREELS in the 120–1350 K surface temperature range [9]. $N_2H_4$ was found to be partially dissociated into $N_2H_x$ ($x = 2$, 3) species with the N-N bond parallel or nearly parallel to the surface at 120 K at a low dosages (e.g. less than 0.2 L). This was evidenced by the appearance of the Si-H vibration at 255 meV in the high-resolution electron-energy-loss spectra and by the relatively larger full widths at half-maximum of the N 1s XPS and the $n^+$, $n^-$ molecular UPS peaks. When an approximately 0.4 L $N_2H_4$ dosed sample was annealed to about 500 K, significant desorption of the molecule occurred as well as further dissociation of the N-H bonds. Above 600 K, the N-N bond began to break. Further annealing of the sample caused complete cracking of the N-H bonds until $Si_3N_4$ was formed. The major processes involved in the reactions of $N_2H_4$ at different temperatures were supposed to be [9]

$$N_2H_4(g) + Si(111) \xrightarrow{120\,K} N_2H_x(a) + H(a)$$
$$\xrightarrow{600\,K} N_2H_x(a) + NH_x(a) + H(a)$$
$$\xrightarrow{650\,K} NH_x(a) + N(a) + H(a)$$
$$\xrightarrow{700\text{-}1000\,K} N(a) \xrightarrow{1350\,K} Si_3N_4(s).$$

Theoretical study of the above processes is absent, but highly appealing owing to the potential industrial application of the above processes for the production of $Si_3N_4$ film.

### 3.5. *$HN_3$/Si(100)*

Bu and co-workers [10] first reported the experimental studies of $HN_3$ ($DN_3$) adsorption and decomposition on the single crystal Si surfaces Si(110) and Si(100), using HREELS, UPS, XPS and Auger electron spectroscopy (AES) at temperatures between 120 and 1350 K. At a low temperature ($T_s \sim 120$ K), $HN_3$ was found to adsorb molecularly on the surface as evidenced by the HN-NN stretching vibration at 1234 $cm^{-1}$, the HNN=N stretching vibration at 2194 $cm^{-1}$ and the H-$N_3$ stretching vibration at 3347 $cm^{-1}$. Upon warming to 220 K, $HN_3$ started to dissociate into $N_2$ and NH, which further dissociated to give N and H as the surface was annealed from 580 to 800 K. The presence of H adatoms was evidenced by the appearance of the Si-H stretching vibration at 2154 $cm^{-1}$. H adatoms were observed to desorb as $H_2$ at $T_s > 800$ K. The adsorption of hydrazoic acid ($HN_3$) on Si(100)-$2 \times 1$ was also studied by Jonathan *et al.* [108] using TPD and AES. The TPD experiments revealed that the desorption products from the $HN_3$-covered Si substrate are molecular $H_2$ and $N_2$. The phenomenon was interpreted by assuming that the adsorption of $HN_3$ on the Si(100) surface is dissociative, yielding NH(a) and $N_2$(a) adspecies. They suggested the $N_2$ species was end bonded to a Si atom. AES revealed the formation of a silicon nitride film upon heating the $HN_3$-covered Si substrate. The experimental work by both groups demonstrated that $HN_3$ is a more efficient nitriding agent for Si than ammonia or hydrazine is.

To elucidate the reaction mechanism behind their experimental observations of the $HN_3$/Si system, Luo *et al.* [109] conducted a first-principle density functional study recently using a double-dimer $Si_{15}H_{16}$ cluster model. Their calculations were performed predominantly at the B3LYP/6-31G(d) level of theory. Several stable adsorption states were found, among which a side-on adsorption state containing a five-membered ring $Si_2N_3$-H surface species and a dissociative adsorption state that consists of Si-H and Si-$N_3$ surface species are the most favourable. The geometries and adsorption energies of the two favourable adsorption states are shown in figure 7. The formation of the five-membered ring $Si_2N_3$-H surface species was predicted to be barrierless, following the famous 1,3-dipolar cycloaddition (1,3-DC) mechanism [110] in organic chemistry. Similar pericyclic 1,3-DC reactions were predicted theoretically to be facile for a series of 1,3-dipole molecules on the C(100) [111] and Si(100) [112] surfaces. On the other hand, the barrierless dissociative adsorption of $HN_3$ on the Si=Si dimer site reminds us of an organic reaction between $HN_3$ and ethylene that forms ethyl azide [113]. Further decomposition of the Si-$N_3$ surface species and the five-membered ring $Si_2N_3$-H

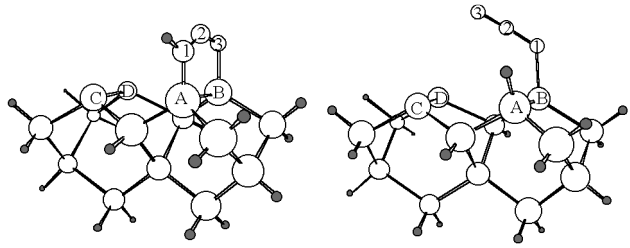


Figure 7. Two favourable adsorption states of $HN_3$ on the Si(100) surface predicted at the B3LYP/LANL2DZ level of theory using a double-dimer $Si_{15}H_{16}$ surface model. The predicted adsorption energies (in kilocalories per mole) are given in parentheses.

surface species leads to $N_2$ elimination accompanied by the formation of a Si-N=Si surface species and a three-membered ring $Si_2N$-H surface species respectively. The latter two surface species would be precursors for further formation of Si nitride films.



### 3.6. *$HN_3$/Si(111)*

Bu and co-workers [11, 12] studied the reaction of hydrozoic acid with the Si(111)-7 × 7 surface using AES, HREELS, UPS and LEED in the temperature range from 120 to 1350 K. $HN_3$ was found to adsorb molecularly on the surface at 120 K, with the formation of dimers at higher dosages (2.0 L or above). At 270 K, $HN_3$ began to decompose into HN and $N_2$ species as indicated by the changes in the NH vibration mode in HREELS and the chemical shift of the N 1s XPS peak. Between 300 and 800 K, the NH species further decomposed into H and N on the surface with the elimination of $N_2$. In this temperature range, the steady increase in the $SiN_x$ and Si-H peaks were noted and LEED exhibited a weak (1 × 1) pattern. When the surface was annealed at $T_s > 800$ K, H(a) recombined to desorb as $H_2$, with N remaining as the only species on the surface. Further annealing at higher temperatures caused the gradual transformation of the $SiN_x$ species into $Si_3N_4$, as confirmed by an (8 × 8) LEED pattern. Bu and co-workers suggested the following mechanism for $HN_3$ reaction with the low-Miller-index Si surfaces:

$$HN_3 \xrightarrow{T_s=100\,K} HN_3(a),$$

$$HN_3(a) \xrightarrow{T_s>270\,K} NH(a) + N_2(g)/HN_3(g),$$

$$NH(a) \xrightarrow{T_s=270\text{-}800\,K} N(a) + H(a),$$

$$2H(a) \xrightarrow{T_s>800\,K} H_2(g),$$

$$Si(s) + N(a) \xrightarrow{T_s>1000\,K} Si_3N_4(s).$$

## 4. The reactions of CO-containing molecules

### 4.1. *CO/Si(100) and CO/Si(111)*

The interaction of CO with Si single-crystal surfaces is of fundamental interest [13–15, 114–125], as CO is a widely used probe molecule in surface science. Dylla *et al.* [114] found that CO molecules penetrate into Si substrates upon adsorption at room temperature and stick more strongly on O-etched surfaces than on polished surfaces. Similarly, a CO desorption signal could be easily detected by dosing O on Si substrates [115]. For CO on the Si(111) surface, Joyce and Neave [116] detected a C signal with AES. In a low energy ion scattering experiment, Onsgaard *et al.* [117] reported that CO readily adsorbed on Si(111), where O, instead of C, could be easily detected. On the contrary, Bu and Lin [13] found that below 100 K and for dosage conditions of a few langmuirs, CO did not exhibit any observable change in HREELS on the Si(111)-$7 \times 7$ surface. The result obtained by Bu and Lin implied that CO was not adsorbed on the Si(111)-$7 \times 7$ surface at all.

For CO on the Si(100)-$2 \times 1$ surface, Bu and Lin [13] first reported the vibrational spectrum of the adsorbed CO using HREELS. Two distinct absorption peaks which appeared at 411 and 2081 $cm^{-1}$ were observed at 100 K and were assigned to the Si–CO stretching mode and to the SiC═O stretching mode, respectively. The low Si–CO stretching frequency as well as the small red shift of the C═O stretching frequency from its free molecular value of 2145 $cm^{-1}$ indicates that the interaction between CO and the Si surface is weak and implies that the CO molecule adsorbs on Si(100)-$2 \times 1$ in an upright, end-on position. Their TPD measurements revealed a desorption peak at 180 K. The main features of their CO/Si(100)-$2 \times 1$ results have been confirmed later by Young *et al.* [123], including the effectiveness of ultraviolet irradiation on the desorption of the CO. Interestingly, using a high-energy 1.3 eV molecular beam of CO in their HREELS experiment at $T_s = 85$ K, Hu *et al.* [124] recently observed two CO stretching modes at 1702 and 2105 $cm^{-1}$ and demonstrated that the 1702 $cm^{-1}$ mode is a non-thermally accessible phase of CO on the Si(100) surface.

Using a $Si_9H_{12}$ cluster model, Hu *et al.* [124] also performed density functional and Hartree–Fock calculations, which revealed two stable sites on the Si surface: the T-CO phase (one CO terminally bound to one Si of each dimer) and the bridge-bound B-CO phase (one CO symmetrically bound to both Si atoms of the dimer). They concluded that the thermal CO molecule leads to the T-CO phase while the translationally high-energy CO leads to the B-CO phase. Imamura *et al.* [125] performed first-principles molecular dynamics calculations with a slab model for the CO/Si(100) system and found two adsorption structures of CO on the Si(100) surface. One is where the CO adsorbed symmetrically with adsorption energy of 17 kcal $mol^{-1}$ and the other asymmetrically with 19 kcal $mol^{-1}$ adsorption energy. The calculated adsorption energies are much larger than the experimental activation energy for desorption [124].

More detailed *ab initio* molecular orbital and hybrid DFT calculations were carried out recently to investigate the adsorption of CO on the Si(100)-$2 \times 1$ surface using two single-dimer cluster models ($Si_9H_{12}$ and $Si_{13}H_{20}$) and a double-dimer cluster model ($Si_{15}H_{16}$) [14, 15]. Figure 8 presents the energy profile of the CO/$Si_9H_{12}$ model system obtained at the B3LYP/6-31G(d) level of theory. It can be seen, firstly, that the CO normal (or T-CO phase) structure is more stable than the CO bridge (or B-CO phase) structure and, secondly, that the formation of the CO-normal adsorbate occurs without a reaction barrier. At the same level of theory using a

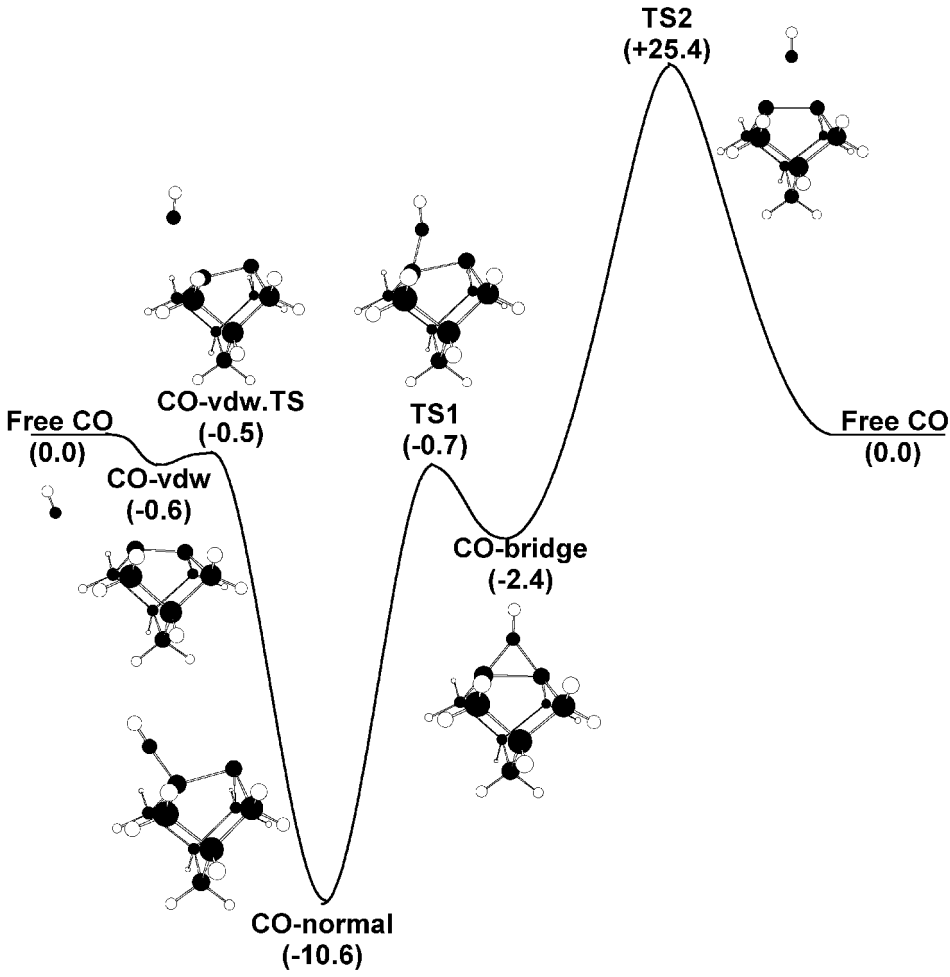


Figure 8. Profile of energy surface for the $CO/Si_9H_{12}$ model system predicted at the B3LYP/6-31G(d) level of theory. The relative energies (in kilocalories per mole) are given in square brackets.

scaled factor of 0.97, the predicted C═O stretching frequency is 1755 $cm^{-1}$ for the OC-bridge mode, while for the OC-normal mode, the predicted Si–CO stretching mode and SiC═O stretching mode frequencies are 455 and 2071 $cm^{-1}$, respectively, in good agreement with the HREELS observation. So far as the bonding mechanism is considered, detailed NBO analyses on the wavefunctions of the model systems revealed that in the OC-normal adsorption mode, a dative bond is formed between the lone pair at the C atom (mostly 5σ characteristic) and the empty antibonding $\pi^*$ orbital of the surface dimer that is mostly localized on the buckled-down Si atom. As a result, the CO lone pair donates charge into the surface dimer and the occupied π orbital of the surface dimer is mostly localized on the buckled-up Si atom, which prohibits the adsorption of a second CO on the same surface dimer. Using a double-dimer $Si_{15}H_{16}$ cluster model, Bacalzo-Gladden and Lin [15] have further investigated the adsorbate–adsorbate interaction and found, firstly, that one surface dimer can accommodate no more than one CO molecule chemically and, secondly, that the

adsorbate–adsorbate interaction is rather weak due to the large dimer–dimer separation (about 4.2 Å).

Kinetic modelling of the thermal desorption of CO [126] was performed employing the RRKM theory [79–82] with the computed energetics and the following general mechanism for the OC-normal adsorbate:

$$N_{(a)} \xrightarrow{1} CO + Si_{(s)}$$

$$\underset{-2}{\overset{2}{\rightleftharpoons}} B_{(a)} \xrightarrow{3} CO + Si_{(s)}$$

where $N_{(a)}$ and $B_{(a)}$ represent the OC-normal and OC-bridge adsorbates respectively. Because the isomerization of these structural isomers is posssible, in principle, the reversible isomerization reactions (2) and (−2) are included in our calculations. It should be noted that under thermal conditions, the concentration of $B_{(a)}$ is too low to be detected by HREELS [13, 123, 124]. The predicted rate constant for the thermal desorption of OC-normal adsorbate is

$$k_N = 2.83 \times 10^{13} \exp\left(\frac{-11\,000}{RT}\right) s^{-1},$$

where $R = 1.987\,\text{cal}\,\text{mol}^{-1}\,\text{K}^{-1}$. Figure 9 shows the calculated desorption rate constant together with that reported by Hu *et al.* [124]. The theory agrees reasonably well with experiment in terms of the absolute values of the rate constant. For this one-step, simple desorption process, our calculated frequency factor of $2.8 \times 10^{13}\,s^{-1}$ supports the value typically assumed in the modelling of TPD data based on the Redhead [127] method (with $1 \times 10^{13}$) and our B3LYP/6-31G(d) desorption energy of $10.6\,\text{kcal}\,\text{mol}^{-1}$ agrees well the desorption energy of $11.5\,\text{kcal}\,\text{mol}^{-1}$ estimated by

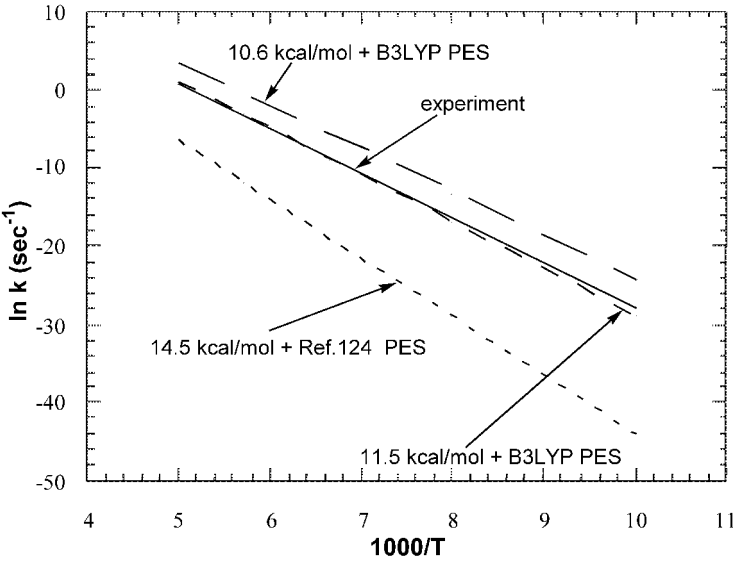


Figure 9. Arrhenius plot of the desorption rate constant of N-CO on the Si(100)-2 × 1 surface in the temperature range 100–200 K (PES, potential energy surface): (——), line based on the frequency factor and activation barrier reported by Hu *et al.* [124].

Hu *et al.* [124] in their molecular-beam experiment. For comparison, the calculated desorption energy of 14.5 kcal mol$^{-1}$ by Hu *et al.* at the B3P86/6-31G(d, p) level was also used in our RRKM calculations; the rate constant thus obtained is in poor agreement with their experimental value, as shown in figure 9.

### 4.2. *$CH_2O$/Si(100) and $CH_3CHO$/Si(100)*

To the best of our knowledge, no experimental work can be found in the literature concerning the formaldehyde reaction with the Si(100) surface. Armstrong *et al.* [128] have studied the thermal interactions of acetone and acetaldehyde on Si(100), both sputtered and annealed, using high HREELS, XPS and TPD. No carbonyl stretching mode was detected by HREELS and the C and O 1s XPS peaks reflected two different carbonyl processes, one involving bond cleavage, and the other a reduction in the C-O bond order. SiO was found to desorb near 1050 K and XPS shows total loss of O and retention of C. Approximately 34% of the acetaldehyde monolayer and 62% of the acetone monolayer decomposed on annealed Si(100) to produce silicon carbide. They concluded that Si dimers play an important role in the chemistry of carbonyl groups, which was recently confirmed by our first principles density functional calculations regarding the chemisorption of $CH_2O$ on the Si(100)-$2 \times 1$ surface [16].

Figure 10 shows the equilibrium geometry for $CH_2O$ adsorption on the Si dimer optimized at the B3LYP/6-31G* level of theory [16]. Formaldehyde chemisorbs with its carbonyl group being di-σ-bonded on to the Si dimer, giving rise to the formation of a close four-membered -SiCOSi- ring. Upon chemisorption, the C-O bond in $CH_2O$ and the Si-Si bond of the Si dimer are elongated by 0.25 and 0.12 Å respectively. The geometrical change indicates the chemisorption-induced reduction of bond order of the C-O bond and of the Si-Si dimer. Such a [2 + 2] cycloaddition process is exothermic and barrierless, proceeded by a nucleophilic attack of the O end of formaldehyde on to the positively charged buckled-down Si atom of the Si-Si

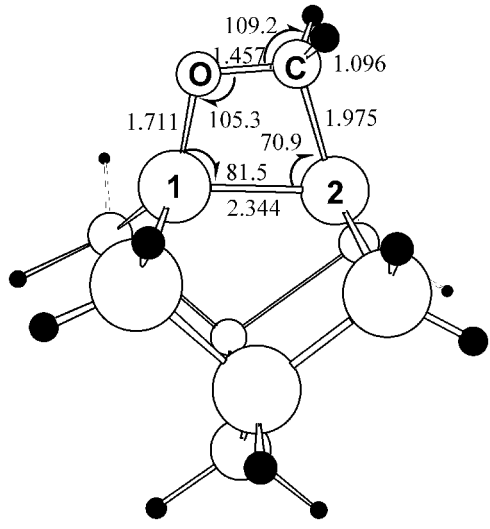


Figure 10. Equilibrium geometry (bond distances in ångströms) for $CH_2O$ adsorption (energies in kilocalories per mole) on the $Si_9H_{12}$ surface model predicted at the B3LYP/6-31G(d) level of theory. (From [16]. Reproduced by the permission of the Royal Society of Chemistry.)

dimer. The predicted chemisorption energy is $-48.9\,\text{kcal mol}^{-1}$ at the B3LYP/6-31G* level. Further single-point, two-layered ONIOM(CCSD(T)/6-31G(d):B3LYP/6-31G(d)) calculations predicted a chemisorption energy of $-42.2\,\text{kcal mol}^{-1}$, which is several kilocalories per mole lower than the B3LYP/6-31G(d) prediction. The vibrational frequencies of adsorbed and free $CH_2O$ were also computed. The C-O bond stretching frequency shows a significant red shift from 1778 to $953\,\text{cm}^{-1}$ upon chemisorption. Meanwhile, the C-H bond stretching frequencies of the $CH_2$ group shift from $2850\,\text{cm}^{-1}$ (asymmetric $CH_2$ stretch) and $2800\,\text{cm}^{-1}$ (symmetric $CH_2$ stretch); this is typical of $CH_x$ species with an $sp^2$ C atom, to 2979 and $2931\text{cm}^{-1}$, which are typical of $CH_x$ species with an $sp^3$ C atom respectively. Such considerable shifts of C-O and $CH_2$ stretch frequencies can be fingerprints of the di-σ-bonded $CH_2O$ in experimental vibrational analysis of the $CH_2O$/Si(100) system.

Moreover, this study provides the first theoretical evidence that similar to the cycloaddition of formaldehyde to ethylene that leads to the formation of oxetane [129], a C=O bond can also undergo [2 + 2] addition on to the Si-Si dimer of the Si(100)-2 × 1 surface. Apart from the present formaldehyde study, it was theoretically demonstrated that molecules containing groups of multibonds, such as C≡C (e.g. $C_2H_2$ [17,130–132]), C=C (e.g. $C_2H_4$ [132]), C=N (e.g. phenyl isothiocyanate [133]), C≡N (e.g. HCN [18, 19]), N=N (e.g., $HN_3$ [109] and azo-*tert*-butane [134]) and N=C=S (e.g. phenyl isothiocyanate [133]) can undergo cycloaddition reactions on the Si(100) surface, giving rise to di-σ-bonded surface species. It is a fascinating and noteworthy feature that the Si-Si dimer of the Si(100)-2 × 1 surface is facile to undergo cycloaddition with adsorbates containing double or triple bonds; this opens up ways to functionalize Si surfaces in a specific desired pattern and, hence, may be one of the keys to making usable molecular wires and new molecule-scale devices.



### 4.3. *$CH_2O$/Si(111) and $CH_3CHO$/Si(111)*

Neither experimental nor theoretical work has been reported to date regarding formaldehyde on the Si(111)-7×7 surface. The thermal stability of acetaldehyde on the Si(111)-7 × 7 surface was studied by Bu *et al*. [20] with HREELS, XPS, UPS and TPD techniques. Acetaldehyde molecules were found to adsorb molecularly on the surface at 120 K, yielding HREELS peaks at 98, 124, 144, 185 and 380 eV and UPS peaks at 5.7, 7.6, 10.0, and 13.9 eV below $E_F$. Analysis of the XPS O 1s (shoulder at 531 and 532 eV) and C 1s (288 and 285 eV) spectra indicated that the acetaldehyde was partially dissociated at 120 K. At about 350 K, the initial HREELS peaks at 185 and 144 meV diminished while peaks at 100 and 208 meV emerged, which indicated the desorption and/or dissociation of the C-C bond and the formation of Si-O and Si-$CH_3$ species. The UPS peaks at 5.7 and 10.0 eV diminished, and a new peak at 6.5 eV dominated the spectra from 350 to 1150 K. The parent mass was found by TPD to desorb at 320 K. At 500 K, the 100 meV HREELS peak vanished and a new peak at 270 meV became noticeable, indicating the breaking of the C-H bond and the formation of Si-H (D) species. TPD results indicated that H (D) species desorbed at around 800 K. By 1150 K, peaks at about 110 meV (HREELS) and about 7 eV (UPS) were the only significant features not found in the clean Si(111) spectra. In the X-ray photoelectron spectra, initial multiple features had converged by 350 K, and with increased temperature both the resulting O 1s and C 1s peaks shifted towards lower binding energies. By 1150 K, the O 1s peak disappeared, leaving silicon carbide

on the substrate. No theoretical study of the $CH_3CHO$/Si(111) chemisorption system has been found in the literature.

### 4.4. *$CH_2CO$/Si(111) and $CH_2CO$/Si(100)*

The adsorption and thermal decomposition of ketene ($CH_2CO$) on the Si(111)-$7 \times 7$ surface were investigated using various surface analysis techniques [21]. When the surface was exposed to ketene at 120 K, two CO stretching modes at 220 and 273 meV appeared in HREELS, corresponding to two adsorbed ketene states. After the sample was annealed at 250 K, the 273 and the 80 meV peaks vanished, indicating the disappearance of one of the adsorption states by partial desorption of the adsorbate. In a corresponding TPD measurement, a desorption peak for ketene species was noted at 220 K. Annealing the sample at 450 K caused the decomposition of the adsorbate, producing $CH_x$ and O adspecies. Further annealing of the surface at higher temperatures resulted in the breaking of the CH bond, the desorption of H and O species and the formation of silicon carbide. The desorption of H at 800 K was confirmed by the appearance of the $D_2$ ($m/e = 4$) TPD peak at that temperature when $CD_2CO$ was used instead of $CH_2CO$.

Ketene contains both C═C and C═O double bonds. Similar to the chemisorption of ethylene ($C_2H_4$) on the Si(111) surface [135], either the C═C or the C═O groups of ketene may undergo cycloaddition reaction with the diradical-like rest-atom–adatom pair presenting on the Si(111)-$7 \times 7$ surface, giving rise to two types of adspecies that are di-σ-bonded on to the surface atoms either through two Si-C bonds or through a Si-C bond and a Si-O bond respectively, as schematically shown in figure 11. It can be speculated that upon thermal activation, the C-C bond in the configuration in figure 11 (*a*) would be cleaved to form $CH_2$ adspecies with the elimination of CO, whereas the C-O bond in the configuration in figure 11 (*b*) may be broken to produce $CCH_2$ and O adspecies. Further theoretical work is required to confirm such a possibility.

No prior work has been found concerning $CH_2CO$ adsorption on the Si(100)-$2 \times 1$ surface. It has been known that organic molecules containing either the $>C{=}C<$ group or the $>C{=}O$ group can undergo facile [2 + 2] cycloaddition with the surface Si dimers, forming four-membered ring surface species [16, 132]. However, the relative reactivities of the two types of functional group towards the surface dimer are not known so far. Accordingly, whether $CH_2CO$, which contains both functional groups, would be attached on the surface dimer selectively with one of the functional groups is a question of fundamental interest. In other words, $CH_2CO$ can be a good probe molecule to clarify the relative reactivities of the two groups towards the surface dimers on the Si(100)-$2 \times 1$ surface. In this regard, more elaborate experimental and theoretical investigations are needed.

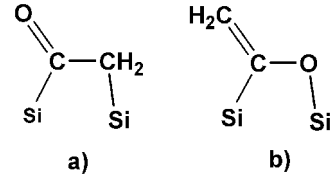


Figure 11. Possible bonding configurations of $CH_2CO$ adsorbed on the rest-atom–adatom pair site presenting on the Si(111)-$7 \times 7$ surface.

### 4.5. *$CH_3OH$/Si(100)*

Deuterated methanol adsorption on the Si(100)-$2 \times 1$ surface has been investigated by synchrotron radiation photoemission and photostimulated desorption at room temperature [136]. Photoemission experiments as a function of methanol coverage showed that deuterated methanol adsorption is dissociative on the surface and occurs via σ(O-D) bond breakage and σ(Si-O) bond formation [136]. The reaction of methanol with both porous Si- and H-covered porous Si was investigated by means of Fourier transform infrared (FTIR) spectroscopy [137], which revealed that that adsorption of methanol on to porous Si at 300 K resulted in cleavage of the O-H bond and formation of Si-$OCH_3$ and Si-H surface species, and heating of these surface species to about 500 K caused the breakage of both the C-O and the C-H bonds. Similar results were obtained in the experimental studies of ethanol adsorption on the Si(100) surface [138, 139] and porous Si [140]. A recent vibrational study of ethanol adsorption on the Si(100) surface confirmed theoretically the adsorption-induced formation of Si-$OC_2H_5$ surface species by means of *ab initio* cluster calculations [138].

Theoretical investigation of the $CH_3OH$/Si(100)-$2 \times 1$ chemisorption system was carried out by Lu *et al.* [16] using a single-dimer $Si_9H_{12}$ cluster model at the B3LYP/6-31G(d) level of theory and at the two-layered ONIOM(CCSD(T)/6-31G(d):B3LYP/6-31G(d)) level of theory. In particular, in the two-layered ONIOM calculations, the high-level part consisting of the adsorbate, the Si-Si dimer and the added H atoms were treated at the CCSD(T)/6-31G(d) level [141] of theory. The thus-obtained profile of energy surface for the $CH_3OH/Si_9H_{12}$ model system is depicted in figure 12. It shows that the dissociative adsorption of methanol on the Si(100) surface takes place readily, giving rise to Si-$OCH_3$ and Si-H surface species, that is a dissociative state DS in figure 12. The reaction, occurring in a barrierless way via a precursor state PS and a transition state TS, is highly exothermic. The reaction enthalpy is predicted to be $-67.9\,\mathrm{kcal\,mol^{-1}}$ at the B3LYP/6-31G(d) level and $-64.7\,\mathrm{kcal\,mol^{-1}}$ at the two-layered ONIOM level. Furthermore, it is interesting to find that the energetics predicted at the B3LYP/6-31G(d) level agrees reasonably with that predicted by the two-layered ONIOM(CCSD(T)/6-31G(d):B3LYP/6-31G(d)) calculations, as shown in figure 12.

### 4.6. *$CH_3OH$/Si(111)*

The adsorption of methanol on the Si(111)-$(7 \times 7)$ was found to be dissociative at rather low temperatures by means of STM, UPS and XPS techniques [136, 142–146]. The EELS experiment at room temperature [142] and the STM experiment [143] revealed that, at room temperature, dissociative adsorption of methanol took place, yielding methoxy species bound to Si surface atoms, while partial formation of a methanol multilayer occurred at low temperature. Photoemission experiments performed by Carbone *et al.* [136, 144] showed that the dissociative adsorption of deuterated methanol on the Si(111)-$7 \times 7$ surface occurs via σ(O-D) bond breakage and σ(Si-O) bond formation, similar to that occurring on the Si(100)-$2 \times 1$ surface. Detailed valence-level and core-level photoemission spectra [145] indicated that methanol adsorption leads to a strongly selective extinction of the rest-atom feature in the valence-level photoemission spectrum, and that, in the Si 2p core-level photoemission spectrum, the $S_2$ surface state related to the rest atoms is quickly quenched upon low coverage adsorption, whereas the $S_1$ surface state partially related to the adatoms is quenched only subsequently at much higher coverages. The

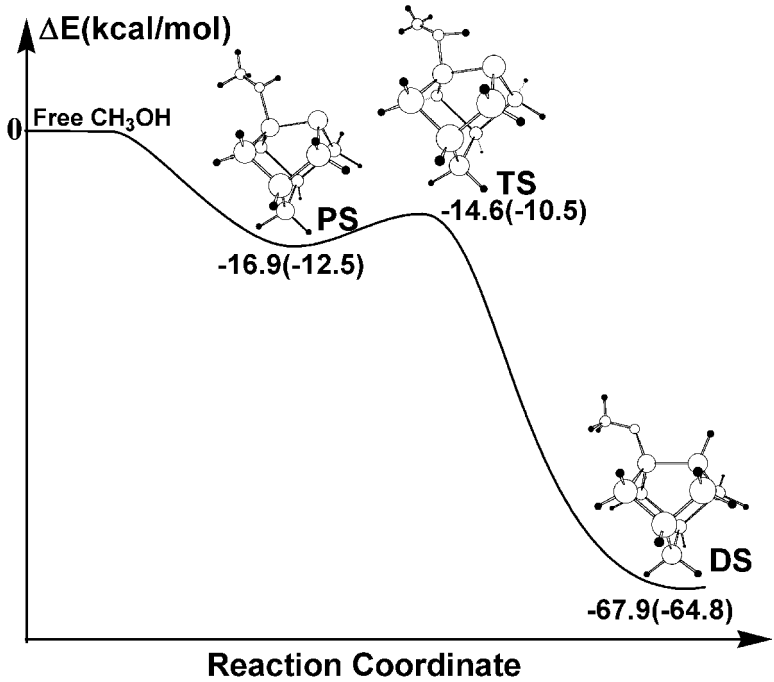


Figure 12. Energy profile for the reaction pathway of $CH_3OH$ chemisorbed on the Si(100)-$2 \times 1$ surface predicted at the B3LYP/6-31G(d) level of theory. The data given in parentheses are obtained by two-layered ONIOM(CCSD(T)/6-31G(d):B3LYP/6-31G(d)) calculations. (From [16]. Reproduced by the permission of the Royal Society of Chemistry.)



intriguing photoemission phenomena led to a seemingly reasonable conclusion that the reactivity of the rest atom is higher than that of the adatoms towards methanol and the methoxy species is preferentially bonded to the rest atoms, as proposed by Piancastelli *et al.* [145]. Arguments given below will show that the intriguing photoemission phenomena are not fully supportive of such a conclusion.

According to the DAS model of the Si(111)-$7 \times 7$ surface, there are six rest atoms, 12 adatoms and a corner-hole atom within a unit cell of the surface, which contribute totally 19 dangling bonds with 19 electrons. Previous electronic structure calculations [101–103] suggested that the dangling-bond states at the six rest atoms and the corner-hole atom are occupied, while the dangling-bond states at the 12 adatoms are fractionally occupied. This means that, with a $7 \times 7$ unit cell, the sum of valence electrons associated to the dangling-bond states at the 12 adatoms should be far fewer than 12*e*. The dissociative adsorption of a methanol molecule consuming a rest-atom–adatom pair site should in principle quench an occupied dangling-bond state at a rest atom and an empty state at an adatom, irrespective of which of the two surface atoms is occupied by the methoxy and the H adspecies. When all the rest atoms are consumed by adspecies, all of the occupied surface states related to the rest atoms are quenched; meanwhile, the empty surface states related to the adatoms to be reacted are quenched, while those partially occupied surface states related to the unreacted adatoms are not quenched at all. Note that only those occupied states can be detected in the photoemission experiments. It is not surprising that, in the valence-level photoemission experiments, the photoemission peaks attributed to

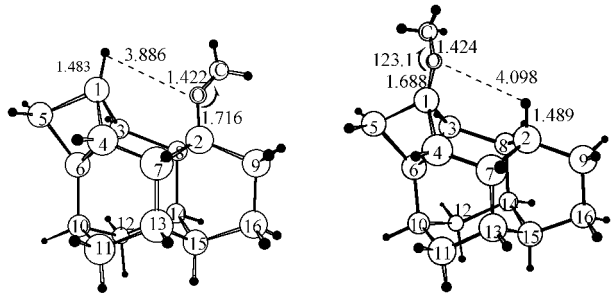


Figure 13. Optimized geometries (bond distance in ångströms) and adsorption energies (in kilocalories per mole) for the dissociative adsorption of methanol over a rest-atom–adatom pair site on the Si(111)-7 × 7 surface predicted by density functional B3LYP calculations (Si, H, LANL2DZ; C, O, 6-31+G*).



the surface states at the rest atoms are quenched quickly at the initial stage of methanol adsorption, while the photoemission band owing to the surface states at the adatoms seems intact. In short, such intriguing phenomena do not essentially mean that the reactivity of the rest atoms is higher than that of the adatoms towards methanol but simply is convincing evidence for the involvement of the rest atoms in the dissociative adsorption of methanol. Furthermore, the preferential charge transfer from the rest atoms to the adatoms [101–103] implies that, on the Si(111)-7 × 7 surface, the rest atoms and adatoms would be basic and acidic sites respectively. This means that the dissociative adsorption of methanol might give rise to methoxy species attached preferentially to the adatoms and H attached on the rest atoms.

First-principles density functional calculations using a $Si_{16}H_{18}$ surface model have been carried out to investigate the dissociative adsorption of methanol over a rest-atom–adatom pair site within the faulted half of a 7 × 7 unit cell [146]. The results showed that the dissociative adsorption is barrierless and highly exothermic with no specific site preference, that is methanol dissociation on the rest-atom–adatom pair site can be initiated by attacking either the rest atom or the adatom with its O atom. NBO analyses indicated that charge transfer between the two dangling bonds at the rest atom and at the adatom is facile and unexpectedly significant even at a large methanol–Si distance (e.g. 3.1 Å), accounting for the site non-preference of methanol dissociation over the rest-atom–adatom pair site. The optimized geometries and adsorption energies for the dissociative adsorption of methanol on the pair site are presented in figure 13.

### 4.7. *HCOOH/Si(100)*

The adsorption of formic acid on the Si(100) surface was investigated by means of HREELS [147], photo-simulated ion desorption [148] and surface near-edge X-ray absorption fine structure (NEXAFS) [149] techniques. The HREELS experiment [147] revealed that formic acid was partially dissociated to form the unidentate formate (HCOO) species and H adatoms on the Si surface at 90 K, and then, it was molecularly adsorbed to form a condensed HCOOH multiplayer on the formate-covered Si(100) surface. The condensed HCOOH layer was removed by heating at

200 K. By heating at about 600 K, the unidentate formate adspecies was decomposed predominantly into SiOSi and SiC species, while less than 10% of the unidentate formate species was decomposed into CO and $CO_2$. Exposing the formate-covered Si(100) to atomic H at 350 K led to the formation of methylendiolate ($H_2COO$) adspecies. The $H_2COO$ surface species thus obtained can be thermally decomposed predominantly into SiOSi and SiC species at 800 K [147]. Recent NEXAFS measurements by Ikeura-Sekiguchi and Sekiguchi [149] suggested such an adsorption structure for formic acid on the Si(100) surface that formic acid is dissociated into H adatom and formate adspecies each occupying one Si atom site of a surface dimer, and the CDO group of the surface chemisorbed formate (Si-OCDO) is tilted away from the surface normal by an average angle of $21 \pm 2^{\circ}$.

Theoretical investigations of the HCOOH/Si(100)-$2 \times 1$ chemisorption system were carried out by Lu *et al.* [16] using a single-dimer $Si_9H_{12}$ cluster model at the B3LYP/6-31G(d) level of theory and at the two-layered ONIOM(CCSD(T)/6-31G(d):B3LYP/6-31G(d)) level of theory. The calculations predicted two possible dissociative reaction pathways for HCOOH on the Si(100) surface, as presented in figure 14. The first route, similar to that of the dissociation of $CH_3OH$ on the same surface site, proceeds via a weakly adsorbed precursor state PS1 and a transition state TS1 and results in a dissociative chemisorption state DS1, which consists of a unidentate formate and a Si-H surface species. The second route proceeds in a barrierless concerted way so that, together with the formation of the Si-O bond between the buckled-down Si atom and the carbonyl O atom of HCOOH, the cleavage of the hydroxyl O-H bond by the buckled-up Si atom occurs simul-



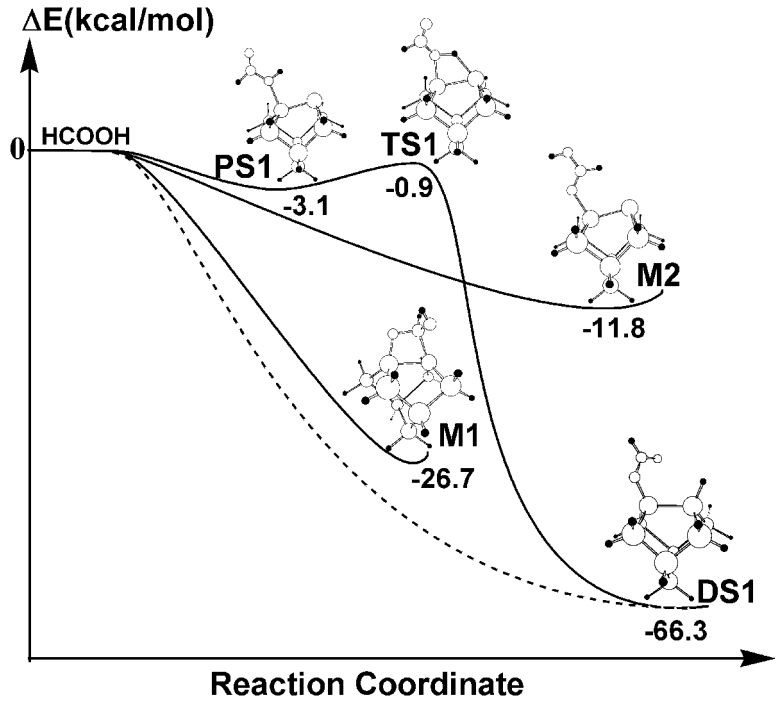


Figure 14. Energy profile for the reaction pathway of HCOOH chemisorbed on the Si(100)-$2 \times 1$ surface predicted at the B3LYP/6-31G(d) level of theory.

taneously, leading to DS1. Therefore, whether there are a precursor state and a transition state in the first route is not important at all for the dissociative adsorption of HCOOH. The dissociation process is highly exothermic with a reaction enthalpy of $-66.3\,\mathrm{kcal\,mol^{-1}}$ predicted at the B3LYP/6-31G(d) level and $-61.9\,\mathrm{kcal\,mol^{-1}}$ predicted at the ONIOM(CCSD(T)/6-31G(d): B3LYP/6-31G(d)) level of theory. In DS1, the thus-formed Si-O and Si-H bond lengths are 1.744 and 1.490 Å respectively. The HCOO-Si species is nearly planar with its HCOO plane tilted away from the surface normal by about 23°. This prediction confirms the recent experimental estimation [149] that the molecular plane of the adsorbed formate group is tilted away from surface normal by an average angle of $21 \pm 2°$.

Apart from PS1 and DS1, two other molecular adsorption states M1 and M2 were found in the calculations, as depicted in figure 14. M1 is formed by [2 + 2] cycloaddition of the C=O group on to the Si-Si dimer. Its formation energy is predicted to be $-26.7\,\mathrm{kcal\,mol^{-1}}$ at the B3LYP/6-31G(d) level and $-21.9\,\mathrm{kcal\,mol^{-1}}$ at the ONIOM(CCSD(T)/6-31G(d):B3LYP/6-31G(d)) level. M2 is a physisorption state in which HCOOH is weakly attached on to the buckled-down Si atom through the carbonyl O atom. The binding energy of M2 is $-11.8\,\mathrm{kcal\,mol^{-1}}$ predicted at the B3LYP/6-31G(d) level of theory. As such, either M1 or M2 is not predominant in the HCOOH/Si(100) system.



### 4.8. *HCOOH/Si(111).*

The adsorption and decomposition of formic acid on the Si(111) surface was studied by HREELS [147]. It was found that similar to that occurring on the Si(100) surface formic acid was partially dissociated to form unidentate formate adspecies and H adatoms at 90 and 300 K. The unidentate formate adspecies on Si(111) can be further decomposed into SiOSi and SiC species by heating at about 550 K [147]. Reasonable speculation can be made that the dissociation of formic acid occurs over a rest-atom–adatom pair site on the Si(111)-$7 \times 7$ surface, giving rise to the HCOO(a) and H(a) adspecies. Note that on the same pair site the dissociative adsorption of $H_2O$, which has a stronger H-O bond than has HCOOH, readily occurs at a low temperature.

## 5. The reactions of CN-containing molecules

The interaction of CN-containing molecules with the Si surface is practically relevant to the chemical vapour deposition of $SiCN_x$ films which have been shown to exhibit crystalline texture and a wide bandgap [7, 22–24].

### 5.1. *HCN/Si(100)*

Bu *et al.* [25] reported the adsorption and thermal reaction of HCN (DCN) on the Si(100)-$2 \times 1$ using UPS, XPS and HREELS. At dosages greater than 4 L and lower surface temperatures ($T_s = 100$ K), HCN formed dimers and polymers on Si(100). After annealing the sample to 220 K, CN and HCNH adspecies were identified. The former showed a peak at 263 meV attributable to the C≡N stretching vibration, while the latter exhibited peaks at 160, 368 and about 400 meV for the HC=NH, CH and NH stretching vibrations respectively. The adsorbed CN, denoted CN(a), appeared to undergo reorientation from the end-on to the side-on configuration when the sample was annealed at 560 K. Above 680 K, the dissociation of NH and C≡N bonds took place. After the surface was annealed to temperatures

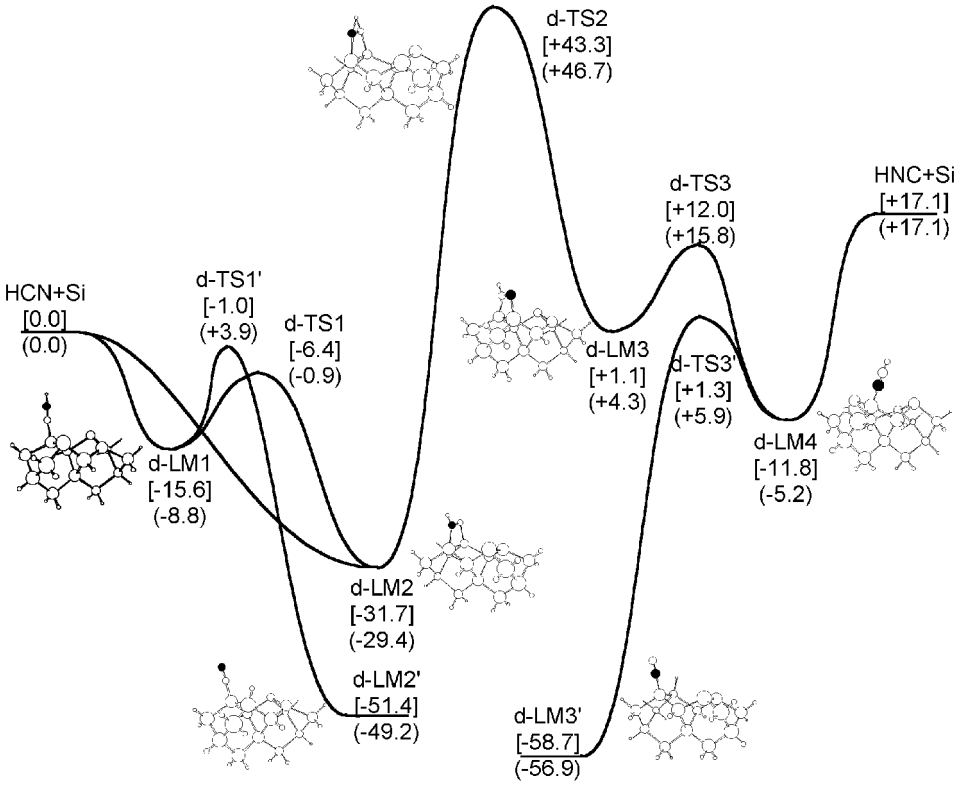


Figure 15. Profile of energy surfaces for the adsorption, isomerization and decomposition of HCN on the Si(100)-2 × 1 surface predicted at the B3LYP/6-31G(d) level of theory. The relative energies (in kilocalories per mole) obtained with the double-dimer $Si_{15}H_{16}$ and single-dimer $Si_9H_{12}$ cluster models are given in square brackets and parentheses respectively. (From [19]. Reproduced by the permission of the American Chemical Society, © 2001.)



greater than 820 K, Si carbide and Si nitride were produced following the decomposition of CH(a) and the desorption of H species.

The adsorption, isomerization and decomposition of HCN on the Si(100)-2 × 1 surface have been investigated by means of DFT calculations using the single-dimer $Si_9H_{12}$ and double-dimer $Si_{15}H_{16}$ cluster models [18, 19]. Figure 15 presents the profile of energy surfaces for the model system computed at the B3LYP/6-31G(d) level of theory. It shows that HCN can be readily adsorbed on a Si═Si dimer either dissociatively or molecularly in an end-on and a side-on configuration. The side-on adsorption d-LM2 occurs by the [2 + 2] cycloaddition of the C≡N group on to the Si═Si dimer; whereas dissociative adsorption d-LM2 gives rise to -H(a) and -CN(a) adspecies initially via the end-on configuration d-LM1 on the same dimer or across the two dimers. Besides those adsorption states shown in figure 15, the DFT calculations have revealed two more adsorption configurations in which HCN is tetra-σ bonded with two surface dimers, as shown in figure 16. Because of their tetra-σ bonding with the substrate atoms, the C-N bond length of the HCN molecule is elongated significantly to 1.46 Å for d_tb1 and to 1.523 Å for d_tb2, indicating that the C-N bond order decreases from 3 to 1. Despite the fact that they are found to be thermodynamically far less favourable than the side-on adsorption state and the

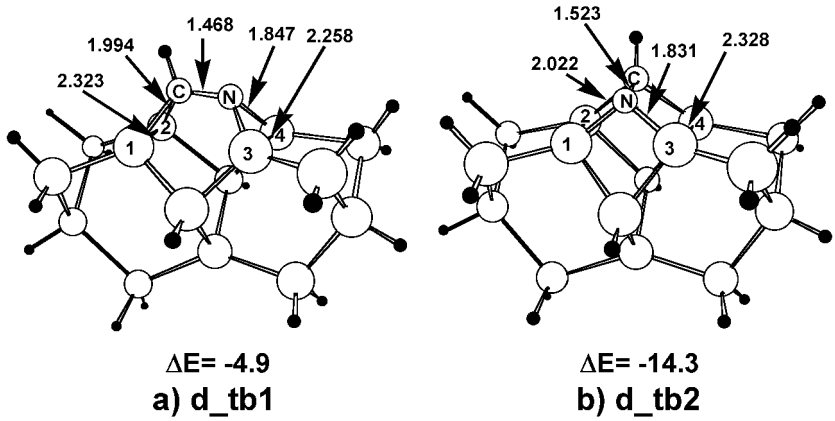


Figure 16. Tetra-σ-bonding configurations of HCN with two surface dimers predicted at the B3LYP/6-31G(d) level of theory. The reported energies (in kilocalories per mole) are relative to free HCN and the free $Si_{15}H_{16}$ cluster model.



dissociative adsorption state on a single dimer site, their multiple σ bonding with four substrate atoms implies that they would be among those possible precursors leading to the formation of a SiCN film.

Adsorbate–adsorbate interactions and reactions have also been studied with two HCN molecules. A synergetic effect has been observed for the parallel adsorption of two HCNs with their C═N groups bridging across the two dimers. For the side-on adsorption, the adsorbate–adsorbate interaction is negligible with a minor effect on the adsorption geometry. H migration between the two neighbouring side-on HCN admolecules can occur readily, leading to the formation of HCNH(a) and NC(a) surface species, as shown in figure 17. The theoretical vibrational frequencies of the HCNH(a) and NC(a) adspecies predicted at the B3LYP/LANL2DZ level of theory are given in table 2, together with the experimental HREELS data extracted from [25]. The agreement of the theoretical prediction with the experimental observation is fairly good.

Table 2. Comparison of calculated HCNH vibrational frequencies using the double-dimer (HCNH.d34) models with experiment.

| | HCNH vibrational frequency ($cm^{-1}$) | | |
|---|---|---|---|
| Mode | Experiment | HCNH.d34 model | HCNH.eb model |
| HCNH(a) species | | | |
| N-H stretch | 3428 | 3514 | 3500 |
| C-H stretch | 3226 | 3178 | 3154 |
| C═N stretch | 1290–1613 | 1498 | 1480 |
| N-H, C-H bend (in plane, asymmetric) | — | 1401 | 1444 |
| N-H, C-H bend (in plane, symmetric) | — | 1193 | 1269 |
| N-H, C-H bend (out of plane, asymmetric) | — | 1046 | 1053 |
| N-H, C-H bend (out of plane, symmetric) | — | 774 | 742 |
| NC (a) species | | | |
| C≡N stretch | 2097–2113 | 2089 | 2086 |

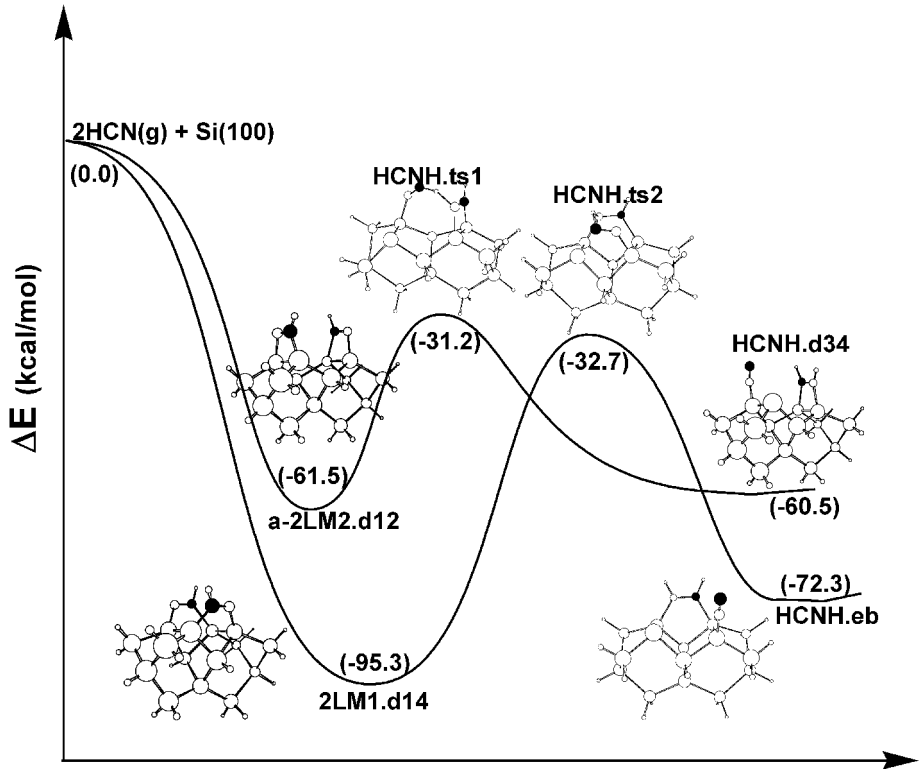


Figure 17. Profile of energy surfaces for the formation of HCNH surface species on the Si(100)-2 × 1 surface predicted at the B3LYP/6-31G(d) level of theory. The relative energies (in kilocalories per mole) are given in parentheses. (From [19]. Reproduced by the permission of the American Chemical Society, © 2001.)



### 5.2. *HCN/Si(111)*

The interaction of HCN (DCN) with Si(111)-7 × 7 was studied with HREELS, UPS and XPS [26]. At 100 K with higher dosages (D > 4 L), HCN (DCN) formed dimers and/or polymers on the surface. Warming the sample to 220 K caused the desorption and dissociation of the HCN species. The CN(a) in an end-on adsorption geometry was identified as the major species which survived up to 600 K on the surface, as indicated by the strong 265 meV peak in HREELS. In contrast, the relative concentration of the HCNH species was far lower than that on the Si(100)-2 × 1 and no significant reorientation of CN(a) was noted below 600 K. The observed difference between the interaction of HCN with Si(111)-7 × 7 and with Si(100)-2 × 1 was attributed to the different topologies of the two surfaces. When the sample was annealed to higher temperatures, dissociation of the CN, CH and NH bonds occurred, followed by the desorption of the H species. Above 820 K, only C and N species remained on the Si(111) surface. So far, no theoretical work has been reported concerning this chemisorption system.

### 5.3. *$CH_3CN$/Si(100)*

The interaction of $CH_3CN$ with the Si(100) surface has not been studied experimentally. Recent DFT calculations [150] predicted two adsorption states for

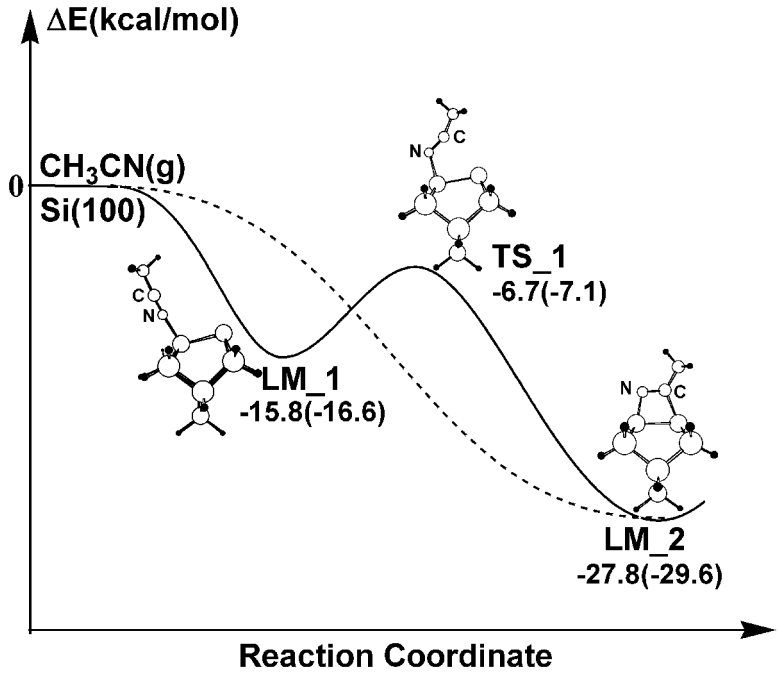


Figure 18. Profile of energy surfaces for $CH_3CN$ adsorption on Si(100) surface predicted at the B3LYP/6-31G(d) level of theory. The relative energies are ZPE corrected, together with the ZPE-uncorrected values given in parentheses. (From [150]. Reproduced by the permission of the Royal Society of Chemistry.)



$CH_3CN$ on a surface dimer modelled by a $Si_9H_{12}$ cluster model, that is an end-on state and a side-on state, as shown in figure 18. In the end-on state, $CH_3CN$ is attached with its N end on to the buckled-down Si atom of the surface dimer. The side-on adsorption state, in which the CN group is di-σ-bonded on to the surface dimer, is formed via a [2 + 2] cycloaddition of the CN group with the Si=Si surface dimer. At the B3LYP/6-31G(d) level, the predicted binding energies are 15.8 kcal mol$^{-1}$ for the end-on adsorption and 27.8 kcal mol$^{-1}$ for the side-on adsorption. As shown in figure 18, configuration transformation from the end-on state to the side-on state has to overcome a barrier height of 9.1 kcal mol$^{-1}$ at TS_1. This does not mean that the formation of the side-on adsorption state has to pass through the end-on adsorption state and the transition state. Detailed potential energy surface scanning calculations revealed that the side-on adsorption state can be formed directly from $CH_3CN$(g) by a side-on approaching route.

### 5.4. *$CH_3CN$/Si(111)*

The molecular adsorption of $CH_3CN$ on the Si(111)-7 × 7 surface has been studied by means of low temperature STM [151]. The STM image for the empty states suggested that the molecular adsorption site might be across the dimer between the faulted and unfaulted halves of the Si(111)-7 × 7 surface. Shirota *et al.* [151] interpreted their STM results by assuming a dipole–dipole interaction between the adsorbate and the surface as well as a molecular adsorption structure so that the methyl and the nitrogen atom are located on top of the faulted centre adatom and

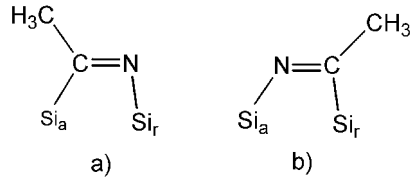


Figure 19. Two di-σ-bonding configurations of $CH_3CN$ adsorbed on the rest-atom–adatom pair site at the Si(111)-7 × 7 surface; $Si_a$, adatom; $Si_r$, rest atom.

the unfaulted centre adatom respectively. However, the assumption of a dipole–dipole interaction between the adsorbate and the surface is in conflict with their observation that upon $CH_3CN$ adsorption, the local density of states for the occupied states decreased at both the unfaulted centre adatom and the faulted centre adatom sites, which implies substantial charge transfer from the surface to the adsorbate and the interaction between the surface and the adsorbate is chemical in nature. The exact adsorption structure of $CH_3CN$ on the Si(111)-7 × 7 surface remains an open question that deserves further experimental and theoretical studies.

It is known that the two dangling bonds available at the rest-atom–adatom pair site on the Si(111)-7 × 7 surface are strongly diradical in nature. Hence, adsorbates, such as $C_2H_2$, $C_2H_4$ and benzene, having multiple bonds can undergo facile cycloaddition reactions with the rest-atom–adatom pair site [135, 152–155], similar to their chemisorptions over the dimer site on the Si(100) surface [17, 132]. On the other hand, the recent DFT study [150] predicted that on the Si(100) a [2 + 2] cycloaddition would occur between the CN group of $CH_3CN$ and the surface dimer, forming di-σ-bonded adspecies. Analogously, one would expect a [2 + 2] cycloaddition of $CH_3CN$ with the rest-atom–adatom pair on the Si(111)-7 × 7 surface. Of course, one should not neglect the possible presence of other adsorption configurations, for example N-end-on adsorption. Such speculations can be easily confirmed theoretically.



### 5.5. *$C_2N_2$/Si(100)*

The adsorption of thermal decomposition of $C_2N_2$ on the Si(100)-2 × 1 surface has been investigated with TPD, XPS, UPS and HREELS [27]. On a sample with $C_2N_2$ (0.5 L) dosed at 100 K, two desorption peaks at 160 and 230 K were noted in the TPD spectrum, presumably deriving from the $C_2N_2$ adsorbed in overlayers and the monolayer respectively. Under lower exposure conditions (less than 0.5 L), only a single broad peak centred at about 250 K was observed. The latter showed C 1s and N 1s XPS peaks at about 1.8 eV lower in binding energy than those of the multilayer $C_2N_2$. The large energy shift in the XPS peaks is probably caused by the strong interaction between the $C_2N_2$ adsorbed side on and the surface at lower coverages. Annealing the $C_2N_2$-dosed Si(100) at about 600 K caused the breaking of the NC–CN bond, and CN adspecies could be identified on the surface. At 700–800 K, CN bond scission occurred, and thus a mixture of Si carbide and Si nitride was formed. The thermal decomposition process for $C_2N_2$ can be summarized as follows:

$$C_2N_2(g) \xrightarrow{100\ K} C_2N_2(a)$$
$$\xrightarrow{<500\ K} C_2N_2(a) + C_2N_2(g)$$
$$\xrightarrow{550\text{-}700\ K} CN(a) + C(a) + N(a)$$
$$\xrightarrow{<800\ K} C(a) + N(a).$$

Preliminary density functional cluster model calculations [156] revealed an end-on adsorption state LM1 and a side-on adsorption state LM2 for $C_2N_2$ on a Si dimer at the Si(100) surface, which is modelled by a single-dimer $Si_9H_{12}$ model. Both adsorption states can be formed in a barrierless manner, as shown in figure 20. In the end-on adsorption state LM1, the linearity of $C_2N_2$ molecule maintains with its N end attached on to the buckled-down Si atom of the Si═Si dimer. In the side-on state, one CN group of the admolecule is di-σ bonded on to the Si═Si dimer, apparently owing to a [2 + 2] cycloaddition of the CN group with the surface dimer. The reacted CN group is nearly parallel with the surface, while the other CN group protrudes away from the surface. The binding energies predicted at the B3LYP/6-



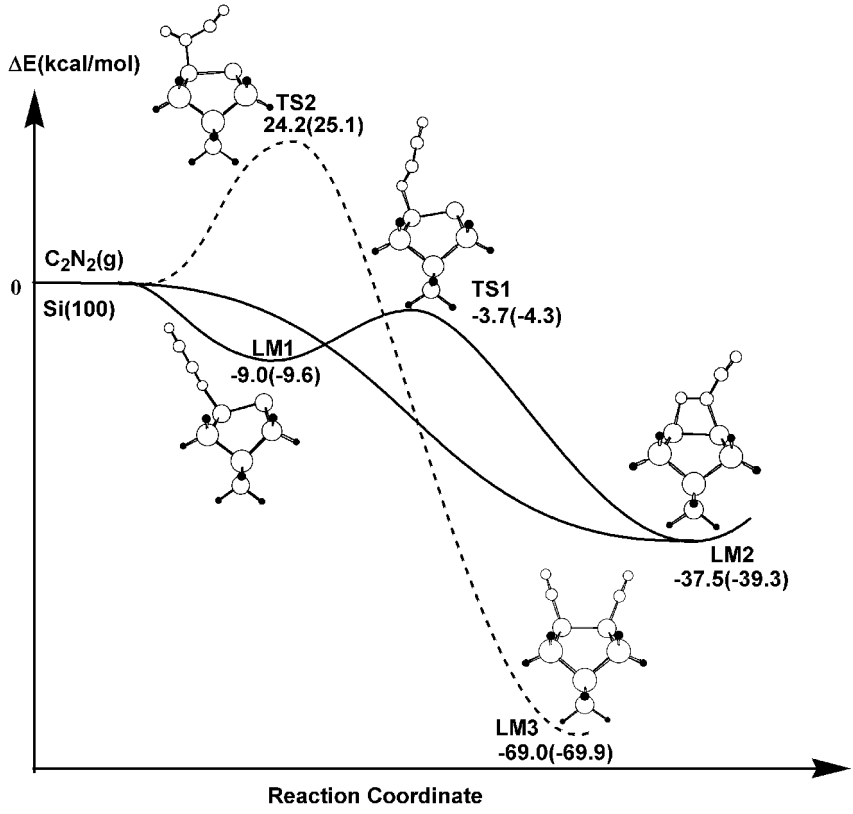


Figure 20. Profile of energy surfaces for $C_2N_2$ adsorption on the Si(100) surface predicted at the B3LYP/6-31G(d) level of theory. The relative energies are ZPE corrected, together with the ZPE-uncorrected values given in parentheses.

31G(d) level of theory are 9.0 kcal mol$^{-1}$ for the end-on adsorption and 37.5 kcal mol$^{-1}$ for the side-on adsorption. On the other hand, a third chemisorption state with two -CN(a) adspecies produced by the NC-CN bond cleavage was found to have a rather high binding energy of 69.0 kcal mol$^{-1}$. However, a reaction barrier of 24.2 kcal mol$^{-1}$ was predicted for such dissociative chemisorption at the B3LYP/6-31G(d) level of theory. Therefore, this state, although thermodynamically favourable over the former two states, cannot be formed at low temperatures as its formation is kinetically forbidden. This state would be a precursor of the thermal decomposition that gives rise to C(a) and N(a) species. Further theoretical study of the decomposition process is in progress using larger cluster models containing two or three surface dimers.

### 5.6. *$C_2N_2$/Si(111)*

The adsorption and thermal decomposition of $C_2N_2$ on the Si(111)-7 × 7 surface were investigated with TPD, XPS, UPS and HREELS [27]. The experimental results are similar to those obtained for the $C_2N_2$/Si(100) system, except that the dissociation of $C_2N_2$ occurred at 550 K on the Si(111)-7 × 7 surface, but at about 600 K on the Si(100) surface. This implies similar chemistry of $C_2N_2$ on both Si surfaces.



### 5.7. *$CH_3N_2H_3$/Si(111)*

The adsorption and thermal decomposition of $CH_3N_2H_3$ on Si(111)-7 × 7 surface were investigated by Bu *et al.* [9] using XPS, UPS and HREELS in the 120–1350 K temperature range. It was partially dissociated into $CH_3N_2H_2$ species with the N-N bond nearly parallel to the surface as it adsorbed on the surface at 120 K. Annealing the dosed surface to about 650 K caused the N-N bond to break, as evidenced by the larger N 1s XPS peak shift, the intensity decrease in the vibrational band in HREELS and the peak shifts in the ultraviolet photoelectron spectra as well. Also there is evidence of minor scission of the C-N bond upon adsorption, including a large C 1s XPS peak shift and additional changes in the ultraviolet photoelectron and high-resolution electron-energy-loss spectra, which becomes more obvious at 730 K. Further cracking of N-H and C-H bonds was found in the $T_s < 800$ K temperature range. Annealing the surface to a higher temperature resulted in the formation of a mixture of silicon nitride and silicon carbide. The major processes involved in the reaction of $CH_3N_2H_3$ at different temperatures can be schematically summarized as follows:

$$\begin{aligned}
CH_3N_2H_3(g) + Si(111) &\xrightarrow{120\ K} CH_3N_2H_x(a) + H(a)\\
&\xrightarrow{<600\ K} CH_3N_2H_x(a) + NH_x(a) + CH_3(a) + H(a)\\
&\xrightarrow{650\ K} CH_xNH_x(a) + NH_x(a) + CH_x(a) + N(a) + H(a)\\
&\xrightarrow{730\text{-}770\ K} CH_x(a) + NH_x(a) + N(a) + H(a)\\
&\xrightarrow{1000\ K} Si_3N_4(s) + SiC(s).
\end{aligned}$$

## 6. The reaction of the NCO-containing molecule $NH_2CHO$

### 6.1. *$NH_2CHO$/Si(100)*

The adsorption and thermal decomposition of $NH_2CHO$ ($ND_2CHO$) on the Si(100)-$2 \times 1$ surface were investigated using HREELS, UPS and XPS [29]. $NH_2CHO$ was found to adsorb randomly on the surface at 100 K and to become ordered, probably with the O atom attached to the surface, when the sample was warmed to 200 K. When the surface was further heated to 450 K, two major reaction pathways were evident: firstly,

$$NH_2CHO(a) \rightarrow OH(a) + HN{=}C(a) \text{ and } H(a)$$

and, secondly,

$$NH_2CHO(a) \rightarrow HNCO(a) + 2H(a).$$

Heating the surface at 550 K caused further desorption and dissociation of the adsorbates, and OH and H species were identified as the major adspecies by HREELS. Above 700 K, a Si-O-Si complex was formed on the surface following the breaking of the OH bonds, while H species desorbed from the surface at $T_s \geqslant 800$ K.

Theoretical study of $NH_2CHO$/Si(100) is absent to date. The $NH_2CHO$ contains both amino ($-NH_2$) and carbonyl ($>C{=}O$) groups. Previous theoretical and experimental studies [8, 9, 16, 51–74] demonstrated that both the $-NH_2$ (e.g. in $NH_3$ and $N_2H_4$) and the $>C{=}O$ (e.g. in $H_2CO$) groups are highly reactive towards the Si=Si dimer abundant on the Si(100) surface. It is thus of fundamental interest to exploit the relative reactivities of the $NH_2$ group and the $>C{=}O$ group towards the surface dimer. For this purpose, $NH_2CHO$, which contains both functional groups is a unique probe molecule.



## 7. The reactions of trimethyl indium

Trimethyl indium (TMIn) can be used as a source of In in organometallic chemical vapour deposition of an InN film on semiconductor surfaces [30–33]. From the mechanistic viewpoint, the reactions of TMIn with Si single-crystal surfaces were studied experimentally [30–32].

### 7.1. *TMIn/Si(111) and TMIn/Si(110)*

The thermal decomposition of TMIn on the Si(111)-$7 \times 7$ surface has been studied using the techniques of XPS, UPS and HREELS [30]. TMIn was found to adsorb molecularly on the surface at 120 K with partial breaking of the $CH_3$ groups from the In atom and an apparent distortion from its original planar geometry in the gas phase. The adsorption-induced distortion of the TMIn molecule is probably caused by the formation of a dative bond between the empty In $5p_z$ orbital and the occupied dangling bond on Si surface atom. The In-C bond cracking continued at 250 K and completed at temperatures above 500 K, giving rise to $CH_3$(a) and In(a) surface species. Further annealing of the sample caused the dissociation of the C-H bonds and desorption of a variety of surface species such as $CH_3$, $CH_2$, In, C, H, etc. At temperatures above 950 K, SiC was the only species detected. Similar adsorption and decomposition behaviours were observed for TMIn on the Si(110) surface [31].

### 7.2. *TMIn/Si(100)*

The adsorption and thermal decomposition of TMIn on the Si(100)-$2 \times 1$ surface was studied with HREELS, XPS and UPS [32]. A molecular adsorption state was observed on the surface at 110 K. A dative bond is probably formed between the empty In $5p_z$ orbital and the dangling bond on the buckled-up Si atom of the Si dimer on the Si(100)-$2 \times 1$ surface, thus inducing a distortion of the TMIn from its original planar structure and possibly partial breaking of the $CH_3$ from the In atom on to the surface. However, the dissociation of the In-C bonds occurred to a less extent than in the case of TMIn on the Si(111)-$7 \times 7$ surface [30]. At 250 K, there were no obvious changes in HREELS except the attenuation of all peaks and, at 520 K, the In-C stretching modes were still visible. Above 520 K, the In-C bond breaking was essentially complete and the cracking of the C-H bonds took place on the surface. At $T_s \geqslant 950$ K, only C was left on the surface following the decomposition of TMIn and desorption of the In and H species. It is thus clear that the Si(100)-$2 \times 1$ surface is less reactive to TMIn than is the Si(111)-$7 \times 7$ surface.

## 8. The reactions of aromatic heterocyclic compounds

Increasing interest in the interaction of aromatic heterocyclic compounds, such as pyrrole ($C_4H_5N$), thiophene ($C_4H_4S$), furan ($C_4H_5O$), pyridine ($C_5H_5N$), etc., with semiconductor surfaces arises from the practical requirement of developing new high-quality polymer- and/or semiconductor-based junctions [157, 158]. Recently, the adsorptions of pyrrole, thiophene, furan, pyridine, pyrazine ($C_4H_4N_2$) and *s*-triazine ($C_3H_3N_3$) on the Si(100)-$2 \times 1$ and the Si(111)-$7 \times 7$ surfaces were studied experimentally and, for some, theoretically [28, 34–37, 159–181].



### 8.1. *Pyrrole/Si(100)*

The XPS and HREELS experiments reported by Qiao *et al.* [159] showed that a steady low-pressure dosing of pyrrole on a Si(100)-$2 \times 1$ substrate at 300 K resulted in the formation of a well-aligned layer of $C_4H_4N$ (*N*-pyrrolyl) adspecies on the surface. The reaction was presumed to take place via the dissociative adsorption of $C_4H_4NH$ by the interaction of the lone-pair electrons on the N atom with the unoccupied orbital in one of the surface Si-dimer atoms:

$$C_4H_4NH + Si\text{-}Si \rightarrow C_4H_4N(a) + H(a) \quad (1)$$

This surface reaction was confirmed by Cao *et al.* [160] using FTIR spectroscopy and XPS. Besides the predominant *N*-pyrrolyl adspecies, Cao *et al.* also observed the presence of di-σ-bonded adspecies presumably formed by further cleaving a $C_\alpha$-H bond of the *N*-pyrrolyl adspecies. In such a di-σ-bonded adspecies, the overall aromaticity of the $C_4N$ ring is preserved. Other di-σ adspecies due to $[2 + 2]$ cycloaddition or $[4 + 2]$ cycloaddition [28], which was observed in the thiophene/Si(100)-$2 \times 1$ chemisorption system [36, 160], were not observed in the pyrrole/Si(100) $-2 \times 1$ system.

The mechanism for the dissociative adsorption of pyrrole producing *N*-pyrrolyl adspecies and H adatoms on the Si(100)-$2 \times 1$ surface was very recently explored by Luo and Lin [34] by means of DFT cluster model calculations. The theoretical study indicated that reaction (1) occurs too slowly under the experimental conditions studied by Qiao *et al.* [159]. Instead, they found that the barrierless addition of the pyrrole molecule at the α-C position to one of the Si-dimer atoms followed by N-H

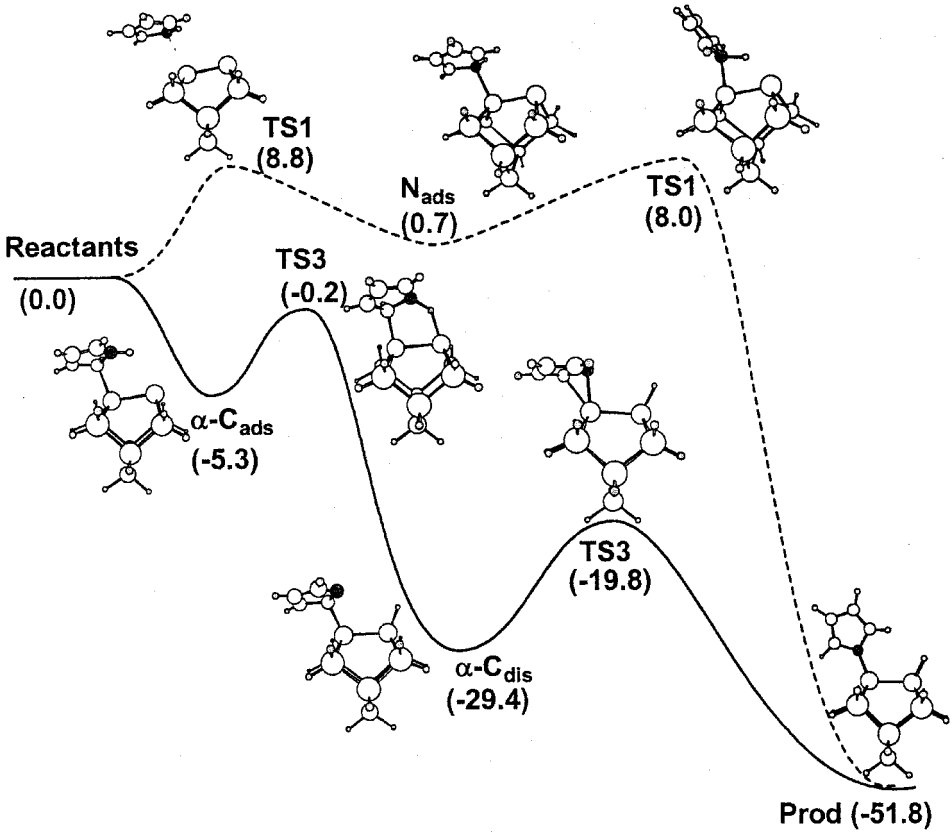


Figure 21. Profile of energy surfaces for the dissociative adsorption of pyrrole on the Si(100)-2 × 1 surface. Geometries optimized at the B3LYP/6-31G(d) level and the relative energies (in kilocalories per mole) predicted at the B3LYP/6-311+G(2df,2p) level of theory. (From [34]. Reproduced by the permission of Elsevier Science.)



dissociation and isomerization of the radical does produce the products given in reaction (1) without thermal activation. Figure 21 demonstrates the reported profile of energy surfaces for the dissociative adsorption of pyrrole on the Si(100)-2 × 1 surface [34]. In addition, molecular adsorption reactions by [4 + 2] and [2 + 2] cycloaddition mechanisms were considered. These cycloadducts were predicted to be short lived at room temperature and should not affect the formation of the aligned $C_4H_4N$ adlayer. Nevertheless, the experimental and theoretical finding that pyrrole can be covalently attached on to the Si(100)-2 × 1 surface in the form of *N*-pyrrolyl demonstrates a possible way to attach chemically the conductive or semiconductive pyrrole-based polymers on the semiconductor surface.

### 8.2. *Pyrrole/Si(111)*

The only experimental investigation concerning the adsorption of pyrrole on the Si(111)-7 × 7 surface was reported by Macpherson *et al.* [162], who found no detectable TDS profile for pyrrole or lower mass fragments on either the 7 × 7 surface or amorphous surface for room-temperature exposure. This implies that pyrrole does not readily adsorb on the Si(111)-7 × 7 surface. Given the π conjugation

and the relatively weak N-H bond of pyrrole, it is rather difficult to understand why the [4 + 2] cycloaddition of pyrrole or the N-H bond cleavage could not occur on Si(111)-7 × 7 surface, which has more reactive dangling bonds than the Si(100) surface has. Therefore, more elaborate experimental and theoretical investigations are required regarding the interaction of pyrrole with the Si(111) surface.

### 8.3. *Thiophene/Si(100) and furan/Si(100)*

The adsorbed state of thiophene on the Si(100)-2 × 1 was first investigated by Jeong *et al.* [163] using LEED, AES and UPS. The (2 × 1) LEED pattern at 300 K was sustained after saturated exposure of thiophene, and the saturation coverage was estimated to be about 0.6 by AES, suggesting that thiophene molecules are chemisorbed molecularly on the Si(100) surface most probably by σ bonds between C and Si atoms. The ultraviolet photoelectron spectrum for the chemisorbed thiophene showed not only the π orbital shift but also the σ orbital shift. These workers also performed semiempirical PM3 cluster model calculations to study the chemisorption mechanism and proposed that thiophene is di-σ-bonded on to a surface dimer with its 2,3 C atoms, that is a [2 + 2] cycloaddition mechanism [163]. This proposal was contradicted very recently by Qiao *et al.* [161], who studied the same surface reaction by means of UPS, XPS and HREELS. They concluded that thiophene is chemisorbed in the form of a 2,5-dihydrothiophene-like species following a [4 + 2] cycloaddition mechanism. In their experiments, two adsorption states were identified at 120 K and assigned to physisorbed thiophene and chemisorbed thiophene respectively. The physisorbed thiophene desorbs below 200 K. Above 400 K, the chemisorbed species were found either to desorb molecularly or to decompose possibly via α-thiophenyl and Si-H through a H-abstraction mechanism, and via a metallocyclic-like intermediate and atomic S through a S-abstraction mechanism. Whether thiophene undergoes [2 + 2] cycloaddition-like or [4 + 2] cycloaddition-like chemisorption on the Si(100)-2 × 1 is controversial.

So far neither experimental nor theoretical work could be found in the literature regarding furan adsorption on the Si(100)-2 × 1 surface. One infers that the adsorptive behaviour of furan on the Si(100)-2 × 1 surface would be similar to that of thiophene, considering their similarity in geometric and electronic structures.

The chemisorption and decomposition of thiophene and furan on the reconstructed Si(100)-2 × 1 surface have been investigated by means of the hybrid density functional (B3LYP) method in combination with a cluster model approach. Two chemisorption mechanisms, namely [4 + 2] and [2 + 2] cycloadditions of $C_4H_4X$ (X = S or O) on to a surface dimer site, have been considered comparatively. The calculations revealed that the former process is barrierless and favourable over the latter, which requires a small activation energy (2.6 kcal mol$^{-1}$ for thiophene and 1.2 kcal mol$^{-1}$ for furan). Figure 22 shows the profile of energy surfaces for thiophene (furan) chemisorption and decomposition over a double-dimer $Si_{15}H_{16}$ surface model predicted at the B3LYP/6-31G(d) level of theory. As shown in figure 22, the di-σ-bonded surface species LM1_d or LM1_d′ formed by [4 + 2] cycloaddition-type chemisorption can undergo either further [2 + 2] cycloaddition with a neighbouring Si=Si dimer site, giving rise to a tetra-σ-bonded surface species LM3_d, or deoxygenation/desulphurization by transferring the heteroatom to a neighbouring Si=Si dimer site, leading to a six-membered ring metallocyclic $C_4H_4Si_2$ surface species LM4_d. The latter process was found to be slightly more favourable than the former, especially in the case of thiophene.

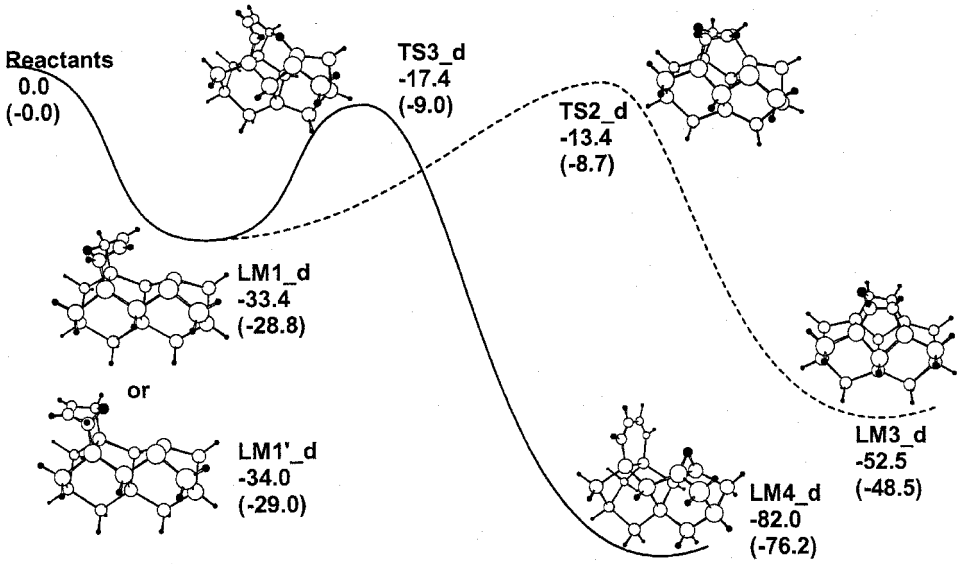


Figure 22. Profile of energy surfaces (in kilocalories per mole) for thiophene (furan) chemisorption and decomposition over a double-dimer $Si_{15}H_{16}$ surface model predicted at the B3LYP/6-31G(d) level of theory. (From [36]. Reproduced by the permission of the American Chemical Society, © 2001.)



### 8.4. *Thiophene/Si(111)*

The thermal desorption profiles of thiophene on Si(111)-7 × 7 were obtained for room-temperature exposure [162, 164]. Two molecular desorption peaks were observed at 350 K (weak) and 405 K (intensive) from the Si surface, indicating two bonding states of thiophene for the room temperature adsorption. It was proposed that the first state corresponds to a π-bonded ring-planar geometry while the second involves the lone-pair electrons of S atom in a σ-bonded ring-perpendicular geometry. This was seemingly supported by photoemission experiment with monochromatic synchrotron radiation at 340 eV photon energy, in which two C 1s photopeaks were observed for thiophene adsorbed at room temperature [165]. Very recently, Cao *et al.* [166] studied the dry thienylation of the Si(111)-7 × 7 surface under ultrahigh-vacuum conditions by means of STM and HREELS. They found that the adjacent adatom and rest atom can serve as a diradical for the heterogeneous [4 + 2] cycloaddition reaction between thiophene molecules and the Si(111) surface. The resulting cycloadduct follows a 2,5-dihydrothiophene-like structure with the S atom and the remaining C=C bond tilted from the surface [166]. A similar heterogeneous [4 + 2] cycloaddition reaction was also found for benzene on the Si(111)-7 × 7 surface [154, 155].

The 2,5-dihydrothiophene-like adsorption structure for thiophene adsorbed over the adjacent adatom and rest-atom pair site at the Si(111)-7 × 7 surface was confirmed by our density functional cluster model calculations using a $Si_{16}H_{18}$ surface model [156]. The B3LYP calculations (using LANL2DZ basis sets for Si and H and 6-31+G(d) basis sets for S and C) predicted that the [4 + 2] cycloaddition-like adsorption of thiophene can readily occur at room temperature with an adsorption enthalpy of $-51$ kcal mol$^{-1}$. Considering the strong diradical character of the rest-atom–adatom pair site at the Si(111)-7 × 7 surface, one should not exclude the

possibility of the [2 + 2] cycloaddition reaction between thiophene and the surface. Further theoretical work is being undertaken to show this possibility.

### 8.5. *Furan/Si(111)*

Similar to the case of thiophene, the thermal desorption spectroscopy (TDS) experiment [164] showed two desorption peaks at 355 K (intensive) and 420 K (weak) for room-temperature adsorption of furan on the Si(111)-7 × 7 surface. Accordingly, the two desorption states were assigned to the π-bonded and σ-bonded molecular adsorbates [164]. The XPS experiment [167] detected two C1s photoelectron peaks at room temperature for both room-temperature exposure and exposure at 90 K. However, the very recent TDS and HREELS experiments reported by Cao *et al.* [168] suggested that, besides the [4 + 2] cycloaddition reaction between furan and the surface that produces the 2,5-dihydrofuran-like surface species, dimerization of adsorbed furan that is mediated by the surface dangling bonds would occur on the Si(111)-7 × 7 surface, giving rise to a surface species responsible for the higher-temperature desorption peak in TDS. They also performed semiempirical PM3 cluster model calculations, which indicated that the dimerized adsorption state is about 22 kcal mol$^{-1}$ more stable than the 2,5-dihydrofuran-like state. More elaborate theoretical study is required to confirm their speculation of dangling-bond mediated dimerization of furan on the Si(111)-7 × 7 surface.



### 8.6. *Pyridine/Si(100)*

The adsorption of pyridine ($C_5H_5N$) on the Si(100) surface has not been investigated experimentally yet. Having a N heteroatom, this molecule has a dipole moment of 2.19 D [169] induced by the in-plane lone pair localized at the N heteroatom. Therefore, it may behave differently on the Si(100) surface from its homocyclic analogue, benzene, for which experimental and theoretical studies revealed a butterfly-like di-σ-bonded adspecies on the Si(100) surface [28, 132, 170, 171]. On the other hand, the lone pair at the N heteroatom arms pyridine with the capability of forming a N-to-metal dative bond, as was observed on transition-metal surfaces [172, 173]. Indeed, a recent DFT study [150] showed that pyridine can be adsorbed with its N end on to the buckled-down Si atom of the surface dimer on the Si(100)-2 × 1 surface (figure 23 (*a*)). In addition, two side-on adsorption states, produced by [4 + 2] cycloaddition of pyridine on to a surface dimer, were also found. One is bonded on to the surface dimer through its 1,4 positions, forming a N–Si bond and a C–Si bond (figure 23 (*b*)); another is bonded through its 2,5 positions forming two C–Si bonds (figure 23 (*c*)). The calculations predicted that the side-on adsorption states, although di-σ-bonded, are thermodynamically and kinetically less favourable than the end-on adsorption state that has substantial binding energy (27 kcal mol$^{-1}$ predicted at the B3LYP/6-31G(d) level of theory). This prediction should be significant to the development of a pyridine-based conductive (or semiconductive) polymer film on the Si surfaces, as the pyridine–surface bonding is substantial and, most importantly, does not involve the π states of the conjugated system. It should be mentioned that the adsorption of other aromatic compounds, such as benzene, thiophene and furan, on the Si(100) surface has been shown to destroy inevitably the π conjugation of the aromatic compounds, since the adsorption follows the Diels–Alder cycloaddition mechanism [28, 36, 132]. Destruction of the π conjugation of the aromatic compounds is highly undesirable for the

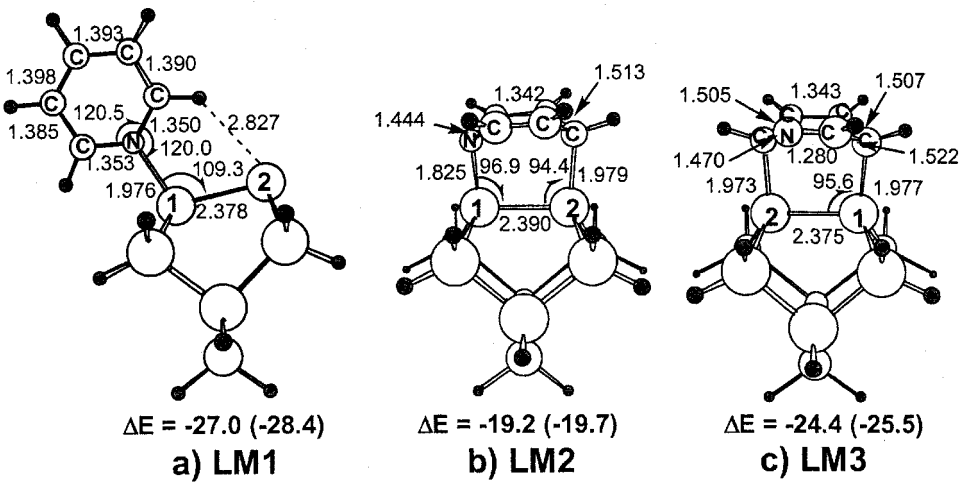


Figure 23. Configurations for the chemisorption of pyridine on the $Si_9H_{12}$ surface model predicted at the B3LYP/6-31G(d) level of theory. The relative energies $\Delta E$ ($kcal\,mol^{-1}$) of these stationary points with respect to free pyridine are also given. The data in parentheses are the ZPE-uncorrected values. (From [150]. Reproduced by the permission of the Royal Society of Chemistry.)



formation of thin films of organic semiconductor polymers on the Si surface [180, 181].

### 8.7. *Pyridine/Si(111)*

The adsorption of pyridine on the Si(111)-7 × 7 surface has been studied by means of LEED, TDS and STM techniques [151, 174–176]. A modified 7 × 7 LEED pattern was observed at room temperature for a dosage of 300 L of pyridine to the Si(111)-7 × 7 surface. TDS showed that pyridine adsorbed molecularly on the Si(111)-7 × 7 surface at room temperature, with two molecular desorption states at 380 and about 470 K [176]. The phenomenon resembles those observed for benzene [177, 178], furan and thiophene [162] on the same surface and indicates that the bonding between pyridine and the surface is substantial and chemical in nature.

Very recently, Shirota and co-workers [151, 176] performed a low temperature STM study which confirmed the molecular adsorption of pyridine on the Si(111)7 × 7 surface. At very low coverages, two adsorption states were observed. The first appeared in the STM images of both the filled and the empty states; the local density of states of this adspecies increased seemingly across the dimer row of the Si(111)-7 × 7 surface. Another is invisible in the STM image of the filled state and its local density of states for the empty state seems higher than that of the former adspecies. The latter adspecies was observed as unfixed during the STM scanning, but the former is fixed, implying that the latter is physisorbed and the former is probably chemisorbed. However, Shirota and co-workers [151, 176] interpreted their observation by suggesting a dipole–dipole interaction between the admolecule and the surface.

Preliminary DFT calculations [146] based on a $Si_{16}H_{18}$ cluster modelling a rest-atom–adatom pair site at the faulted half of the Si(111)-7 × 7 unit cell revealed

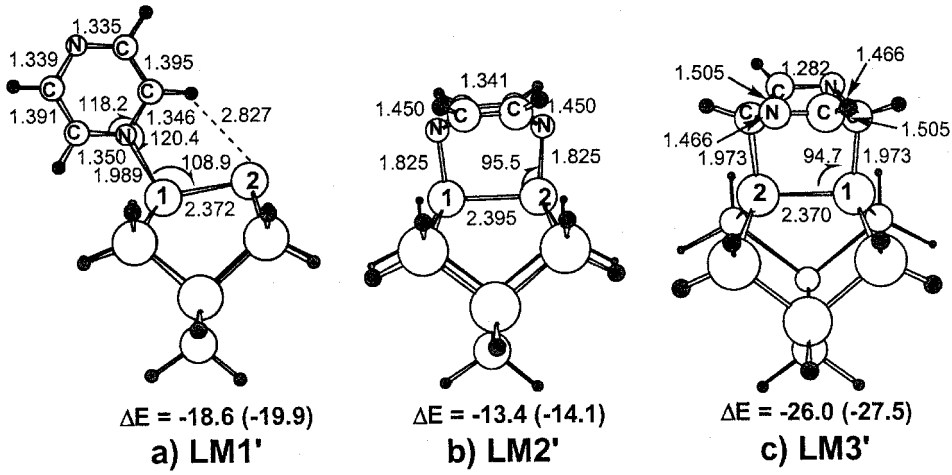


Figure 24. Configurations for the chemisorption of pyrazine on the $Si_9H_{12}$ surface model predicted at the B3LYP/6-31G(d) level of theory. The relative energies $\Delta E$ (kcal mol$^{-1}$) of these stationary points with respect to free pyrazine are also given. The data in parentheses are the ZPE-uncorrected values. (From [150]. Reproduced by the permission of the Royal Society of Chemistry.)



that pyridine readily adsorbs on to the rest-atom–adatom pair site, giving rise to several butterfly-like di-σ-bonded adspecies. Such chemisorptions are analogous to those occurring on Si-Si dimer site of the Si(100)-$2 \times 1$ surface, that is the reaction between pyridine and the rest-atom–adatom pair follows the [4 + 2] cycloaddition mechanism. The predicted binding energies of these adspecies range from 37 to 42 kcal mol$^{-1}$, varying with the location of the N heteroatom. The theoretical study thus reveals the similarity of pyridine and benzene on the Si(111)-$7 \times 7$ surface.

### 8.8. *Pyrazine/Si(100)*

No experimental work has been so far reported regarding the chemisorption of pyrazine on the Si surfaces. Recent DFT cluster model calculations using a $Si_9H_{12}$ surface model predicted that, similar to the pyridine case, pyrazine can be chemisorbed on to the Si-Si dimer site of the Si(100)-$2 \times 1$ surface in three modes, forming an N-end-on adsorption state LM1′ and two side-on adsorption states LM2′ and LM3′, as depicted in figure 24. The binding energies for these three states predicted at the B3LYP/6-31G(d) level are −18.6, −13.4 and −26.0 kcal mol$^{-1}$, respectively. Detailed potential energy surface scanning calculations revealed that the former two states LM1′ and LM2′, although thermodynamically less stable than the latter state LM3′, can be formed in a barrierless way, while the formation of the latter one from gas-phase pyrazine has to overcome a barrier height of 5.2 kcal mol$^{-1}$. The theoretical results suggest that pyrazine would preferentially adopt an end-on adsorption configuration at low temperatures.

### 8.9. s-*triazine/Si(100)*

The thermal decomposition of *s*-triazine ($C_3N_3H_3$) on the Si(100) surface was studied with HREELS, UPS, XPS and TDS [35]. Two desorption peaks at 180 and 235 K were noted in the thermal desorption spectra owing to the overlayer and the monolayer or submonolayer adsorbates, respectively. Above

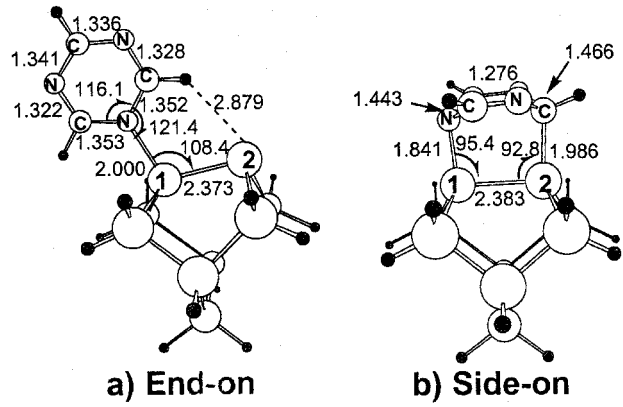


Figure 25. Configurations (bond distances in ångströms, and energies in kilocalories per mole) for the chemisorption of *s*-triazine on the $Si_9H_{12}$ surface model predicted at the B3LYP/6-31G(d) level of theory.



200 K, $C_3N_3H_3$ is likely to lie flat on the surface as indicated by the virtual absence of the asymmetric ring breathing mode at 145 meV in HREELS and by the relatively lower $C_3N_3H_3$ coverage (less than 0.3 L). Annealing the 1.2 L $C_3N_3H_3$-dosed sample at 550 K caused the dissociation of $C_3N_3H_3$ into HC═N, accompanied by the formation of NH and SiH bonds. A further anneal of the surface at 780 K dissociated the CN-containing species and the NH bond. Above 800 K, a mixture of silicon nitride and silicon carbide was formed on the surface following the cracking of the CH bond and the desorption of the H adspecies. The photodissociation of $C_3N_3H_3$ on the Si(100)-2 × 1 surface was also examined [35]. CN radicals and the HCN species could be identified on the surface after it was exposed to 308 nm excimer laser radiation at 100 K. The appearance of CN radicals reflects the difference between the thermal decomposition reaction and the photodissociation process.

Density functional cluster model calculations [156] using a $Si_9H_{12}$ surface model were performed at the B3LYP/6-31G(d) level to investigate the adsorption of *s*-triazine on the Si(100)-2 × 1 surface. Two chemisorption states were revealed in the calculations. The first with a predicted binding energy of 18.2 kcal mol$^{-1}$ is an end-on adsorption state with the formation of a dative bond between the lone pair at the *s*-triazine N atom and the empty antibonding π* orbital localized at the buckled-down Si atom of the surface dimer (figure 25 (*a*)). The second with a predicted binding energy of 25.7 kcal mol$^{-1}$ is butterfly-like and di-σ-bonded on to the surface dimer (figure 25 (*b*)), produced by following the [4 + 2] cycloaddition mechanism. The latter may probably undergo further [2 + 2] cycloaddition with a second surface dimer, giving rise to a tetra-σ-bonded surface species. Analogous tetra-σ-bonded surface species were found in previous theoretical studies regarding the chemisorption of benzene [170, 171], thiophene and furan [36] on the same surface. A further speculation can be made that the tetra-σ-bonded surface species is a precursor state for deep decomposition of adsorbed *s*-triazine. Theoretical modelling of the decomposition process would require a larger cluster model that contains at least two surface dimer sites, for example a double-dimer $Si_{15}H_{16}$ surface model or a triple-dimer $Si_{21}H_{22}$ surface model.

### 8.10. s-*triazine*/*Si(111)*

To the best of our knowledge, the adsorption of *s*-triazine on the Si(111) surface has not be studied so far either experimentally or theoretically. A relevant STM study revealed the non-dissociative adsorption of 2,4,6-triphenyl-1,3,5-triazine (TPT) on the Si(111)-$7 \times 7$ surface [179]. An adsorption structure was assumed in which the three phenyl groups and the central triazine ring lies in a plane flat on the Si surface. It was suggested that a mobile precursor precedes the final molecule surface bonding which is chemisorption in nature and is formed between one N lone-pair orbital of the triazine group and one dangling bond of the Si substrate only [179]. However, this suggestion is questionable with the following considerations. Firstly, the lone-pair orbitals at the N atoms of the triazine ring are localized in the molecular plane. It is impossible to form a dative bond between an in-plane lone pair orbital with a dangling bond at a substrate atom when the TPT plane is parallel to the substrate surface. Secondly, in the case when the TPT plane is perpendicular to the surface in order to fulfil the symmetry requirement for the formation of a $N \rightarrow Si$ dative bond, the two phenyl groups neighbouring the N atom are too spatial to maintain a reasonable N–Si bonding distance. For *s*-triazine without phenyl substituents, the $N \rightarrow Si$ dative bond may be formed when the molecular plane is perpendicular to the substrate surface. On the other hand, it was noted in the previous part of this review that other π-conjugated six-membered ring compounds such as benzene and pyridine preferentially adopt a di-σ-bonded adsorption configuration over the rest-atom–adatom pair site on the Si(111)-$7 \times 7$ surface. Analogously, one would expect similar adsorption states for s-triazine and TPT over the same pair site. To confirm such expectations, further experimental and theoretical work is required.



## 9. Concluding remarks

This article reviews the recent experimental and theoretical studies on the interactions of small [C, N, O]-containing molecules with two representative single crystal surfaces of Si, that is the Si(100)-$2 \times 1$ surface and the Si(111)-$7 \times 7$ surface. Efforts made in these studies are accompanied by the hope of finding an easy and controlled way to produce new superlative Si-based films, for example SiN, SiC, SiCN, SiO and conductive (or semiconductive) polymer/Si films, to be used in microelectronic devices.

Among those nitrogen hydrides considered ($NH_3$, $N_2H_4$ and $HN_3$), $HN_3$ seems to be the best N-precursor molecules for the formation of SiN films, followed by $N_2H_4$ and then by $NH_3$, despite the fact that the latter has been widely used as N precursor for the production of SiN films. The higher reactivity of $HN_3$ to Si surfaces was confirmed by theoretical modelling, which shows that the initial state of $HN_3$ decomposition on Si is quite easy with at least two barrierless reaction pathways.

For CN-containing molecules, HCN seems to be the most reactive toward Si surfaces, followed by $C_2N_2$ and $CH_3CN$, and hence can be a potential CN precursor for the production of SiCN films. $CH_3N_2H_3$, although falling in this group, has the same reactivity as $N_2H_4$ at low and moderate temperatures but leads eventually to a mixture of Si carbide and Si nitride at high temperatures.

The CO-containing molecules, from methanol (alcohol), formaldehyde (aldehyde) to formic acid (carboxylic acid) and ketene, behave differently on the Si surfaces owing to their different functional groups. While molecules containing an

O–H group (e.g. methanol and formic acid) chemisorb dissociatively, molecules containing carbonyl groups (e.g. formaldehyde and ketene) prefer [2 + 2] cycloaddition on a pair of surface atoms. Of particular interest is the adsorption behaviour of ketene, which contains both the C=C and the C=O groups. Although both groups can undergo facile [2 + 2] cycloaddition on to the Si surfaces, a clear-cut assessment of the relative reactivity of the two functional groups toward the Si surface cycloaddition on the surface is absent. Ketene can be a key to answering the question; more elaborate experimental and theoretical studies are appealing.

Similar to ketene, formamide ($NH_2CHO$) also has two functional groups, namely $NH_2$ and C=O, both highly reactive on the Si surface. While the amino group (e.g. in $NH_3$ and $N_2H_4$) can undergo dissociative chemisorption without thermal acitvation, the CO group prefers a barrierless [2 + 2] cycloaddition on Si surfaces. Carefully designed experiments on the adsorption of formamide will be helpful to distinguish the relative reactivities of both groups to the Si surface.

Although the studies regarding the adsorptions of five- or six-membered ring aromatic compounds on the Si surfaces failed to obtain polymer/Si junctions that are highly essential for the production of new microelectronic devices, they did hint at the possibility of forming pyrrole-based (or pyridine-based) conductive (or semiconductive) polymer/Si junctions through covalent Si–N bonding. In this field, several recent successful examples that are not reviewed here are the electropolymerization of polypyrrole thin films on either p-type Si [157] or n-type InP [158] and the formation of a self-assembly of pentacene on the cyclohexene-covered Si(100) surface [180, 181]. Unfortunately, the adhesion thus obtained between the polymer and the semiconductor surface is quite poor owing to weak physical interaction. Therefore, the finding that pyridine and pyrrole can form assemblies on the Si surface through a covalent Si–N bond without destroying the π conjugation of the aromatic ring is indeed encouraging and inspiring for future study in this field.



**Acknowledgements**

The work was supported by Emory University through the Roberts W. Woodruff Professorship. X. L. thanks the Natural Science Foundation of China and Xiamen University for financial support.

*Note added to proof*:—For CN precursors, Mui *et al.* [182] conducted recently a combined MIR-FTIR spectroscopic and DFT study regarding the room-temperature adsorption of methylamine ($CH_3NH_2$), dimethylamine ($(CH_3)_2NH$) and trimethylamine ($(CH_3)_3N$) on the Si(100) surface. Their DFT calculations revealed the following:

(i) the reaction pathways of the amines resemble the precursor-mediated dissociative chemisorption of ammonia;
(ii) the activation barrier for N–$CH_3$ dissociation is significantly higher than that for N–H dissociation, leading to selective cleavage of N–H bonds in the surface reactions of methylamine and dimethylamine as well as trapping trimethylamine in its molecularly chemisorbed state through the formation of a Si–N dative bond.

Their theoretical predictions were confirmed by surface IR studies and were further confirmed by two subsequent theoretical and experimental studies [183, 184]. Meanwhile, Tao *et al.* [185] investigated very recently the adsorption of acetonitrile

on Si(100) by using TPD, XPS and HREELS, and by DFT calculations. This study confirmed our theoretical prediction that acetonitrile chemisorbs on Si(100) in a side-on, di-σ binding configuration, forming Si–C and Si–N bonds.

## References


[1] Waltenburg, H. N., and Yates, J. T. Jr, 1995, *Chem. Rev.*, **95**, 1589.
[2] Hamers, R. J., and Wang, Y., 1996, *Chem. Rev.*, **96**, 1261.
[3] Buriak, J. M., 1999, *Chem. Commun.*, 1051.
[4] Hamers, R. J., Coutler, S. K., Ellison, M. D., Hovis, J. S., Padwitz, D. F., Schwarz, M. P., Greenlief, C. M., and Russell, J. N., Jr, 2000, *Accts. chem. Res.*, **33**, 617.
[5] Wolkow, R. A., 1999, *A. Rev. phys. Chem.*, **50**, 413.
[6] Ekerdt, J. G., Sun, Y.-M., Szabo, A, Szulczewski, G. J., and White, J. M., 1996, *Chem. Rev.*, **96**, 1499.
[7] Chen, L. C., Chen, K. H., Wu, J.-J., Bhusari, D. M., and Lin, M. C., 2001, *Silicon-Based Materials and Devices: Materials and Processing*, Vol. 1, edited by H. S. Nalwa (New York: Academic Press), p. 73.
[8] Bu, Y., and Lin, M. C., 1994, *Surf. Sci.*, **311**, 385.
[9] Bu, Y., Shinn, D. W., and Lin, M. C., 1992, *Surf. Sci.*, **276**, 184.
[10] Bu, Y., Chu, J. C. S., and Lin, M. C., 1992, *Surf. Sci.*, **264**, L151; Chu, J. C. S., Bu, Y., and Lin, M. C., 1992, *Proceedings of the Sixth International Conference on Electronic Materials and Processing* (Baltimore, Maryland: SAMPE), p. 31.
[11] Bu, Y., and Lin, M. C., 1994, *Surf. Sci.*, **301**, 118.
[12] Chu, J. C. S., Bu, Y., and Lin, M. C., 1993, *Surf. Sci.*, **284**, 281.
[13] Bu, Y., and Lin, M. C., 1993, *Surf. Sci.*, **298**, 94.
[14] Bacalzo, F. T., Musaev, D. G., and Lin, M. C., 1998, *J. phys. Chem.* B, **102**, 2221.
[15] Bacalzo-Gladden, F., and Lin, M. C., 1999, *J. phys. Chem.* B, **103**, 7270.
[16] Lu, X., Zhang, Q., and Lin, M. C., 2001, *Phys. Chem. chem. Phys.*, **3**, 2156.
[17] Lu, X., and Lin, M. C., 2000, *Phys. Chem. chem. Phys.*, **2**, 4213.
[18] Bacalzo-Gladden, F., Musaev, D. G., and Lin, M. C., 1999, *J. Chin. chem. Soc. Taipei*, **46**, 395.
[19] Bacalzo-Gladden, F., Lu, X., and Lin, M. C., 2001, *J. phys. Chem.* B., **105**, 4368.
[20] Bu, Y., Breslin, J., and Lin, M. C., 1997, *J. phys. Chem.* B, **101**, 1872.
[21] Bu, Y., and Lin, M. C., 1995, *J. Chin. chem. Soc. Taipei*, **42**, 309.
[22] Bhusari, D. M., Chen, C. K., Chen, K. H., Chuang, T. J., Chen, L. C., and Lin, M. C., 1997, *J. Mater. Res.*, **12**, 322.
[23] Chen, L. C., Yang, C. Y., Bhusari, D. M., Chen, K. H., Lin, M. C., Lin, J. C., and Chuang, T. J., 1996, *Diamond Relat. Mater.*, **5**, 514.
[24] Chen, L. C., Bhusari, D. M., Yang, C. Y., Chen, K. H., Chuang, T. J., Lin, M. C., Chen, C. K., and Huang, Y. F., 1997, *Thin Solid Films*, **303**, 66.
[25] Bu, Y., Ma, L., and Lin, M. C., 1993, *J. phys. Chem.*, **97**, 7081.
[26] Bu, Y., Ma, L., and Lin, M. C., 1993, *J. phys. Chem.*, **97**, 11797.
[27] Bu, Y., Ma, L., and Lin, M. C., 1995, *J. phys. Chem.*, **99**, 1046.
[28] Lu, X., Lin, M. C., Xu, X., Wang, N., and Zhang, Q., 2001, *Phys. Chem. Commun.*, **13**, 1.
[29] Bu, Y., and Lin, M. C., 1994, *Langmuir*, **10**, 3621.
[30] Bu, Y., Chu, J. C. S., and Lin, M. C., 1992, *Mater. Lett.*, **14**, 207.
[31] Bu, Y., Chu, J. C. S., Shinn, D. W., and Lin, M. C., 1993, *Mater. chem. Phys.*, **33**, 99.
[32] Bu, Y., Chu, J. C. S., and Lin, M. C., 1993, *Surf. Sci.*, **285**, 243.
[33] Bu, Y., Ma, L., and Lin, M. C., 1993, *J. vac. Sci. Technol.* A., **11**, 2931.
[34] Luo, H., and Lin, M. C., 2001, *Chem. Phys. Lett.*, **343**, 219.
[35] Bu, Y., and Lin, M. C., 1994, *J. phys. Chem.*, **98**, 7871.
[36] Lu, X., Xu, X., Wang, N., Zhang, Q., and Lin, M. C., 2001, *J. phys. Chem.* B, **105**, 10 069.
[37] Lu, X., Xu, X., Wang, N., Zhang, Q., and Lin, M. C., 2002 (to be published).
[38] Takayanagi, K., Tanishiro, Y., Takahashi, M., and Takahashi, S., 1985, *J. vac. Sci. Technol.* A, **3**, 1502.

[39] Appelbaum, J. A., Baraff, G. A., and Hamann, D. R., 1976, *Phys. Rev.* B, **14**, 588.
[40] Redondo, A., and Goddard, W. A., III, 1982, *J. vac. Sci. Technol.*, **21**, 344.
[41] Tromp, R. M., Hamers, R. J., and Demuth, J. E., 1985, *Phys. Rev. Lett.*, **55**, 1303.
[42] Hamers, R. J., Tromp, R. M., and Demuth, J. E., 1986, *Phys. Rev.* B, **34**, 5343.
[43] Hamers, R. J., Tromp, R. M., and Demuth, J. E., 1987, *Surf. Sci.*, **181**, 246.
[44] Chadi, D. J., 1979, *Phys. Rev. Lett.*, **43**, 43.
[45] Paulus, B., 1998, *Surf. Sci.*, **408**, 195.
[46] Shoemaker, J., Burggraf, L. W., and Gordon, M. S., 2000, *J. chem. Phys.*, **112**, 2994.
[47] Northrup, J. E., 1986, *Phys. Rev. Lett.,* **57**, 154.
[48] Stich, I., Payne, M. C., King-Smith, R. D., Lin, J.-S., and Clarke, L. J., 1992, *Phys. Rev. Lett.*, **68**, 1351.
[49] Hamers, R. J., Tromp, R. M., and Demuth, J. E., 1986, *Phys. Rev. Lett.*, **56**, 1972.
[50] Wolkow, R., and Avouris, Ph., 1988, *Phys. Rev. Lett.*, **60**, 1049.
[51] Bozso, F., and Avouris, Ph., 1986, *Phys. Rev. Lett.*, **57**, 1185.
[52] Avouris, Ph., Bozso, F., and Hamers, R. J., 1987, *J. vac. Sci. Technol.* B, **5**, 1387.
[53] Hlil, E. K., Kluber, L., Bischoff, J. L., and Bolmont, D., 1987, *Phys. Rev.* B, **35**, 5913.
[54] Bozso, F., and Avouris, Ph., 1988, *Phys. Rev.* B, **38**, 3937.
[55] Avouris, Ph., Wolkow, R., Bozso, F., and Hamers, R. J., 1988, *Mater. Res. Soc. Symp. Proc.*, **105**, 35.
[56] Taylor, P. A., Wallace, R. M., Choyke, W. J., Dresser, M. J., and Yates, J. T., Jr, 1989, *Surf. Sci.*, **215**, L286.
[57] Dresser, M. J., Taylor, P. A., Wallace, R. M., Choyke, W. J., and Yates, J. T., Jr, 1989, *Surf. Sci.*, **218**, 75.
[58] Bischoff, J. L., Lutz, F., Bolmont, D., and Kubler, L., 1991, *Surf. Sci.*, **251–252**, 170.
[59] Bischoff, J. L., Lutz, F., Bolmont, D., and Kubler, L., 1991, *Surf. Sci.*, **248**, L240.
[60] Larsson, C. U. S., and Flodström, A. S., 1991, *Surf. Sci.*, **241**, 353.
[61] Fujisawa, M., Taguchi, Y., Kuwahara, Y., Onchi, M., and Nishijima, M., 1989, *Phys. Rev.* B, **39**, 12918.
[62] Takaoka, T., and Kusunoki, I., 1998, *Surf. Sci.*, **412–413**, 30.
[63] Zhou, R. H., Cao, P. L., and Fu, S. B., 1991, *Surf. Sci.*, **249**, 129.
[64] Fattal, E., Radeke, M. R., Reynolds, G., and Carter, E. A., 1997, *J. phys. Chem.* B, **101**, 8658.
[65] Lee, S. H., and Kang, M. H., 1998, *Phys. Rev.* B, **58**, 4903.
[66] Miotto, R., Srivastava, G. P., and Ferrraz, A. C., 1998, *Phys. Rev.* B, **58**, 7944.
[67] Rignanese, G. M., and Pasquarello, A., 2000, *Appl. Phys. Lett.*, **76**, 553.
[68] Miotto, R., Srivastava, G. P., Miwa, R. H., and Ferraz, A. C., 2001, *J. chem. Phys.*, **114**, 9549.
[69] Loh, Z. H., and Kang, H. C., 2000, *J. chem. Phys.*, **112**, 2444.
[70] Widjaja, Y., Mysinger, M. M., and Musgrave, C. B., 2000, *J. phys. Chem.* B, **104**, 2527.
[71] Widjaja, Y., and Musgrave, C. B., 2000, *Surf. Sci.*, **469**, 9.
[72] Queeney, K. T., Chabal, Y. J., and Raghavachari, K., 2001, *Phys. Rev. Lett.*, **86**, 1048.
[73] Xu, X., Kang, S. Y., and Yamabe, T., 2001, *Bull. chem. Soc. Japan.*, **74**, 817.
[74] Lu, X., Bacalzo-Gladden, F., and Lin, M. C., 2002 (to be published).
[75] Becke, A. D., 1993, *J. chem. Phys.*, **98**, 5648.
[76] Lee, C., Yang, W., and Parr, R. G., 1989, *Phys. Rev.* B, **37**, 785.
[77] Frisch, M. J., Trucks, G. W., Schlegel, H. B., Gill, P. M. W., Johnson, B. G., Robb, M. A., Cheeseman, J. R., Keith, T., Peterson, G. A., Montgomery, J. A., Raghavachari, K., Al-Laham, M. A., Zakrzewski, V. G., Ortiz, J. V., Foresman, J. B., Peng, C. Y., Ayala, P. Y., Chen, W., Wong, M. W., Andres, J. L., Replogle, E. S., Gomperts, R., Martin, R. L., Fox, D. J., Binkley, J. S., Defrees, D. J., Baker, J., Stewart, J. P., Head-Gordon, M., Gonzalez, C., and Pople, J. A., 1995, *Gaussian 94*, *Revision B.3* (Pittsburgh, Pennsylvania: Gaussian, Inc.).

[78] Dapprich, S., Komáromi, I., Byun K. S., Morokuma, K., and Frisch, M. J., 1999, *J. molec. Struct.* (*Theochem*), **461–462**, 1.
[79] Baer, T., and Hase, W. L., 1996, *Unimolecular Reaction Dynamics: Theory and Experiments* (Oxford University Press).
[80] Madden, L. K., Moskaleva, L. V., Kristyan, S., and Lin, M. C., 1997, *J. phys. Chem.* A, **101**, 6790.
[81] Diau, E. W., Yu, T., Wagner, M. A. G., and Lin, M. C., 1994, *J. phys. Chem.*, **98**, 4034.
[82] Hsu, C.-C., Mebel, A. M., and Lin, M. C., 1996, *J. chem. Phys.*, **105**, 2346.
[83] Nishijima, M., and Fujiwara, K., 1977, *Solid St. Commun.*, **24**, 101.
[84] Isu, T., and Fujiwara, K, 1982, *Solid St. Commun.*, **42**, 477.
[85] Tanaka, S., Onchi, M., and Nishijima, M., 1987, *Surf. Sci.*, **191**, L756.
[86] Kubler, L., Hlil, E. K., Bolmont, D., and Peruchetti, J. C., 1987, *Thin Solid Films*, **149**, 385.
[87] Kubler, L., Hlil, E. K., Bolmont, D., and Gewinner G., 1987, *Surf. Sci.,* **183**, 503.
[88] Koehler, B. G., Coon, P. A., and George, S. M., 1989, *J. vac. Sci. Technol.* B, **7**, 1303.
[89] Avouris, Ph., and Wolkow, R., 1989, *Phys. Rev.* B., **39**, 5091.
[90] Avouris, Ph., 1990, *J. phys. Chem.*, **94**, 2246.
[91] Gupta, P., Dillion, A. C., Coon, P. A., and George, S. M., 1991, *Chem. Phys. Lett.*, **176**, 128.
[92] Cherif, S. M., Lacharme, J.-P., and Sebenne, C. A., 1991, *Surf. Sci.*, **243**, 113.
[93] Colaianni, M. L., Chen, P. J., and Yates, J. T., Jr, 1992, *J. chem. Phys.*, **96**, 7826.
[94] Chen, P. J., Colaianni, M. L., and Yates, J. T., Jr, 1992, *Surf. Sci.*, **274**, L605.
[95] Colaianni, M. L., Chen, P. J., Nagashima, N., and Yates, J. T., Jr, 1993, *J. appl. Phys.*, **73**, 4927.
[96] Yoshimura, M., Takahashi, E., and Yao, T., 1996, *J. vac. Sci. Technol.* B, **14**, 1048.
[97] Björkqvist, M., Göthelid, M., and Karlsson, U. O., 1997, *Surf. Sci.*, **394**, L155.
[98] Zaibi, M. A., Lacharme, J. P., and Sebenne, C. A., 1998, *Surf. Sci.*, **404**, 206.
[99] Dufour, G., Rochet, F., Roulet, H., and Sirotti, F., 1994, *Surf. Sci.*, **304**, 33.
[100] Björkqvist, M., Göthelid, M., Grehk, T. M., and Karlsson, U. O., 1998, *Phys. Rev.* B, **57**, 2327.
[101] Ezzehar, H., Sonnet, Ph., Minot, C., and Stauffer, L., 2000, *Surf. Sci.*, **454–456**, 358.
[102] Stauffer, L., Van, S., Bolmont, D., Koulmann, J.J., and Minot, C., 1993, *Solid St. Commun.*, **85**, 935.
[103] Ezzehar, H., Stauffer, L., Leconte, J., and Minot, C., 1997, *Surf. Sci.*, **388**, 220.
[104] Foster, J. P., and Weinhold, F., 1980, *J. Am. chem. Soc.*, **102**, 7211; Reed, A. E., Curtiss, L. A., and Weinhold, F., 1988, *Chem. Rev.*, **88**, 899.
[105] Tindall, C., Li, L., Takaoka, O., Hasegawa, Y., and Sakurai, T., 1997, *J. vac. Sci. Technol.* A, **15**, 1155.
[106] Tindall, C., Li, L., Takaoka, O., Hasegawa, Y., and Sakurai, T., 1997, *Surf. Sci.*, **380**, 481.
[107] Luo, H., and Lin, M. C., 2001, unpublished results.
[108] Jonathan, N. B. H., Knight, P. J., and Morris, A., 1992, *Surf. Sci.*, **275**, L640.
[109] Luo, H., Bacalzo-Gladden, F., and Lin, M. C., 2001, unpublished results.
[110] Padwa, A., 1984, *1,3-Dipolar Cycloaddition Chemistry*, Vol. 1 (New York: Wiley).
[111] Lu, X., Xu, X., Wang, N., and Zhang, Q., 2002, *J. org. Chem.* (to be published).
[112] Barriocanal, J. A., and Doren, D. J., 2000, *J. vac. Sci. Technol.* A, **18**, 1959.
[113] Kyba, E.A., 1984, *Azides and Nitrenes: Reactivity and Utility*, edited by E. F. V. Scrien (Orlando, Florida: Academic Press), chapter 1.
[114] Dylla, H. F., King, J. G., and Cardillo, M. J., 1978, *Surf. Sci.*, **74**, 141.
[115] Burton, L. C., 1972, *J. appl. Phys.*, **43**, 232.
[116] Joyce, B. A., and Neave, J. H., 1973, *Surf. Sci.*, **34**, 401.
[117] Onsgaard, J., Heiland W., and Taglauer, E., 1980, *Surf. Sci.*, **99**, 112.
[118] Ibach, H., Horn, K., Dorn R., and Lüth, H., 1973, *Surf. Sci.*, **38**, 433.

[119] Lee, F., Backman, A. L., Lin, R., Gow, T. R., and Masel, R. I., 1989, *Surf. Sci.*, **216**, 173.
[120] Forster, A., and Lüth, H., 1989, *J. vac. Sci. Technol.* B, **7**, 720.
[121] Chamberlain, J. P., Clemons, J. L., and Gillis, H. P., 1992, *Proceedings of the 21st Annual Symposium on Applied Vacuum Science Technology*, Clearwater, Florida, USA, 1992.
[122] Chamberlain, J. P., Clemons, J. L., Pounds A. J., and Gillis, H. P., 1994, *Surf. Sci.*, **301**, 105.
[123] Young, R. W., Brown K. A., and Ho, W., 1995, *Surf. Sci.*, **336**, 85.
[124] Hu, D., Ho, W., Chen, X., Wang S., and Goddard, W. A., III, 1997, *Phys. Rev. Lett.*, **78**, 1178.
[125] Imamura, Y., Matsui, N., Morikawa, Y., Hada, M., Kubo, T., Nishijima M., and Nakatsuji, H., 1998, *Chem. Phys. Lett.*, **287**, 131.
[126] Bacalzo-Galdden, F., Lu, X., and Lin, M. C., 2001, unpublished results.
[127] Redhead, P.A., 1962, *Vacuum*, **12**, 203.
[128] Armstrong, J. L., White, L. M., and Langell, M., 1997, *J. Vac. Sci. Technol.* A, **15**, 1146.
[129] Chen, G. J., and Fu, X. Y., 1995, *J. molec. Struct. (Theochem.)*, **36**, 91.
[130] Liu, Q., and Hoffmann, R., 1995, *J. Am. chem. Soc.*, **117**, 4083.
[131] Imamura, Y., Morikawa, Y., Yamasaki, T., and Nakatsuji, H.,1995, *Surf. Sci.*, **341**, L1095.
[132] Konecný, R., and Doren, D. J., 1998, *Surf. Sci.*, **417**, 169.
[133] Ellison, M. D., and Hamers, R. J., 1999, *J. phys. Chem.* B, **103**, 6243.
[134] Ellison, M. D., Hovis, J. S., Liu, H., and Hamers, R. J., 1998, *J. phys. Chem.* B, **102**, 8510.
[135] Piancastelli, M. N., Motta, N., Sgarlata, A., Balzarotti, A., and De Crescenzi, M., 1993, *Phys. Rev.* B, **48**, 17892.
[136] Carbone, M., Zanoni, R., Piancastelli, M. N., Comtet, G., Dujardin, G., and Hellner, L., 1996, *Surf. Sci.*, **352–354**, 391.
[137] Glass, J. A., Jr, Wovchko, E. A., and Yates, J. T., Jr, 1995, *Surf. Sci.*, **338**, 125.
[138] Eng, J., Jr, Raghavachari, K., Struck, L. M., Chabal, Y. J., Bent, B. E., Flynn, G. W., Christman, S. B., Chaban, E. E., Williams, G. P., Rademacher, K., and Mantl, S., 1997, *J. chem. Phys.*, **106**, 9889.
[139] Casaletto, M. P., Zanoni, R., Carbone, M., Piancastelli, M. N., Abelle, L., Weiss, K., and Horn, K., 2000, *Surf. Sci.*, **447**, 237.
[140] Kim, N. Y., and Laibinis, P. E., 1997, *J. Am. chem. Soc.*, **119**, 2297.
[141] Purvis, G. D., and Bartlett, R. J., 1982, *J. chem. Phys.*, **76**, 1910; Hampel, C., Peterson, K. A., and Werner, H.-J., 1992, *Chem. Phys. Lett.*, **190**, 1; Knowles, P. J., Hampel, C., and Werner, H.-J., 1994, *J. chem. Phys.*, **99**, 5219; Deegan, M. J. O. and Knowles, P. J., 1994, *Chem. Phys. Lett.*, **227**, 321.
[142] Edamoto, K., Kubota, Y., Onchi, M., and Nishijima, M., 1984, *Surf. Sci.*, **146**, L533.
[143] Stroscio, J. A., Bare, S. R., and Ho, W., 1985, *Surf. Sci.*, **154**, 35.
[144] Carbone, M., Piancastelli, M. N., Zanoni, R., Comtet, G., Dujardin, G., and Hellner, L., 1997, *Surf. Sci.*, **370**, L179.
[145] Piancastelli, M. N., Paggel, J. J., Weindel, Chr., Hasselblatt, M., and Horn, K., 1997, *Phys. Rev.* B, **56**, 12737.
[146] Lu, X., unpublished results.
[147] Tanaka, S., Onchi, M., and Nishijima, M., 1989, *J. chem. Phys.*, **91**, 2712.
[148] Ikeura-Sekiguchi, H., and Sekiguchi, T., 1997, *Surf. Sci.*, **390**, 214.
[149] Ikeura-Sekiguchi, H., and Sekiguchi, T., 1999, *Surf. Sci*, **433–435**, 549.
[150] Lu, X., Xu, X., Wu, J., Wang, N., and Zhang, Q., 2002, *New J. Chem.*, **26**, 160.
[151] Shirota, N., Tagi, S., Taniguchi, M., and Hashimoto, E., 2000, *J. vac. Sci. Technol.* A, **18**, 2578.
[152] Weiner, B., Carmer, C. S., and Frenklach, M., 1991, *Phys. Rev.* B, **43**, 1678.
[153] Yoshinobu, J., Fukushi, D., Uda, M., Nomura, E., and Aono, M., 1992, *Phys. Rev.* B., **46**, 9520.

[154] Kawasaki, T., Sakai, D., Kishimoto, H., Akbar, A. A., Ogawa, T., and Oshima, C., 2001, *Surf. Interface Anal.*, **31**, 126.
[155] Wang, Z.H., Cao, Y., and Xu, G.Q., 2001, *Chem. Phys. Lett.*, **338**, 7.
[156] Lu, X., and Lin, M. C., 2001, unpublished results.
[157] Onganer, Y., Saglam, M., Turut, A., Efeoglu, H., and Tuzemen, S., 1996, *Solid-St. Electron.*, **39**, 677.
[158] Lonergan, M. C., 1997, *Science*, **278**, 2103.
[159] Qiao, M. H., Cao, Y., Deng , J. F., and Xu, G. Q., 2000, *Chem. Phys. Lett.*, **325**, 508.
[160] Cao, X., Coutler, S. K., Ellison, M. D., Liu, H., Liu, J., and Hamers, R. J., 2001, *J. phys. Chem.* B, **105**, 3759
[161] Qiao, M. H., Cao, Y., Tao, F., Liu, Q., Deng, J. F., and Xu, G. Q., 2000, *J. phys. Chem.* B, **104**, 11211.
[162] Macpherson, C. D., Hu, D. Q., and Leung, K. T., 1992, *Surf. Sci.*, **276**, 156.
[163] Jeong, H. D., Lee, Y. S., and Kim, S., 1996, *J. chem. Phys.*, **105**, 5200.
[164] Hu, D. Q., Macpherson, C. D., and Leung, K. T., 1991, *Solid St. Commun.*, **78**, 1077.
[165] Macpherson, C. D., and Leung K. T., 1995, *Phys. Rev.* B., **51**, 17 995.
[166] Cao, Y., Yong, K. S., Wang, Z. Q., Chin, W. S., Lai, Y. H., Deng, J. F., and Xu, G. Q., 2000, *J. Am. chem. Soc.*, **122**, 1812.
[167] Letarte, S., Adnot, A., and Roy, D., 2000, *Surf. Sci.*, **448**, 212.
[168] Cao, Y., Wang, Z., Deng, J. F., and Xu, G. Q., 2000, *Angew. Chem., Int. Edn.*, **39**, 15.
[169] *1987, CRC Handbook of Chemistry and Physics*, 68th edition (Boca Raton, Florida: CRC Press).
[170] Lopinski, G. P., Moffatt, D. J., and Wolkow R. A., 1998, *Chem. Phys. Lett.*, **282**, 305.
[171] Wolkow, R. A., Lopinski, G. P., and Moffatt, D. J., 1998, *Surf. Sci.*, **416**, L1107.
[172] Haq, S., and King, D. A., 1996, *J. phys. Chem.*, **100**, 16 957.
[173] Rodriguez, J. A., 1992, *Surf. Sci.*, **273**, 385.
[174] Piancastelli, M. N., Kelly, M. K., Margaritondo, G., Anderson, J., Frankel D. J., and Lapeyre, G. J., 1985, *Phys. Rev.* B, **32**, 2351
[175] MacPherson, C. D., and Leung, K. T., 1995, *Surf. Sci.*, **324**, 202.
[176] Yagi, S., Shirota, N., Taniguchi, M., and Hashimoto, E., 2000, *Surf. Sci.*, **454–456**, 157.
[177] Macpherson, C. D., Hu, D. Q., and Leung, K. T., 1991, *Solid St. Commun.*, **80**, 217.
[178] Hu, D. Q., Macpherson, C. D., and Leung, K. T., 1992, *Surf. Sci.*, **273**, 21.
[179] Günster, J., Dieckhoff, S., and Souda, R., 1998, *Thin Solid Films*, **325**, 24.
[180] Meyer zu Heringdorf, F.-J., Reuter, M. C., and Tromp, R. M., 2001, *Nature*, **412**, 517.
[181] Hamers, R. J., 2001, *Nature*, **412**, 489.
[182] Mui, C., Wang, G. T., Bent, S. F., and Musgrave, C. B., 2001, *J. chem. Phys.*, **114**, 10 170.
[183] Kato, S., Kang, S.-Y., Xu, X., and Yamabe, T., 2001, *J. phys. Chem.* B, **105**, 10 340.
[184] Cao, X., and Hamers, R. J., 2001, *J. Am. chem. Soc.*, **123**, 10 988.
[185] Tao, F., Wang, Z. H., Qaio, M. H., Liu, Q., Sim, W. S., and Xu, G. Q., 2001, *J. chem. Phys.*, **115**, 8563.